The Effect of Fuel Injection Conditions on Combustion Processes in a long stroke Cycle Marine Engine

Kweonha Park *

Posted Date: 22 November 2023

doi: 10.20944/preprints202311.1373.v1

Keywords: long stroke marine engines; combustion process; fuel injection pressure; fuel injection timing; spray angle

Article

The Effect of Fuel Injection Conditions on Combustion Processes in a Long Stroke Cycle Marine Engine

Kweonha Park *

Division of Mechanical Engineering, Korea Maritime and Ocean University, Busan 49112, Korea; khpark@kmou.ac.kr

* Correspondence: khpark@kmou.ac.kr; Tel.: +82-10-9455-5413

Abstract: With growing regulations on ship emissions, specifically carbon dioxide and nitrogen oxides, this study emphasizes the critical need for improving the performance of existing ship diesel engines. Focusing on easily modifiable injection conditions within the fuel system, the research aims to enhance combustion characteristics for operational ships. The study provides a concise analysis of the combustion performance improvements achievable in the field. The study employed a range of calculation conditions, spanning from fuel injection pressures of 20 MPa to 160 MPa, injection timing from 15 degrees before top dead center (BTDC) to 5 degrees after top dead center (ATDC), and spray angles varying between 10 degrees and 50 degrees. A comprehensive analysis was conducted, focusing on fuel distribution behavior, combustion dynamics, carbon monoxide (CO) production and extinction, as well as nitrogen oxide (NO) production. This thorough examination aimed to provide insights into the complex interplay of these factors in order to optimize combustion performance in ship diesel engines. The analysis indicated that substantial unburned fuel occurred at injection pressures below 40 MPa and spray angles less than 20 degrees. This issue was significantly mitigated when injection pressures exceeded 80 MPa or a spray angle of 40 degrees was employed. High flame propagation speeds were observed at injection pressures over 80 MPa and injection timings before BTDC 10. Carbon monoxide emissions were notably low when injection pressures exceeded 80 MPa and a 40-degree spray angle was used. Nitrogen oxide emissions were minimized under conditions of injection pressure below 40 MPa, injection timing after BTDC 5 degrees, and a spray angle between 30 and 40 degrees. The study concludes that the most effective injection conditions for concurrently reducing fuel consumption, minimizing incomplete combustion products, and lowering nitrogen oxide emissions in the target engine are optimal when the injection pressure is set at 80 MPa, the injection timing is positioned at 5 degrees before top dead center (BTDC), and the spray angle is maintained at 40 degrees.

Keywords: long stroke marine engines; combustion process; fuel injection pressure; fuel injection timing; spray angle

1. Introduction

Ships, responsible for transporting 75% of global cargo, emit pollutants like carbon dioxide, nitrogen oxides, sulfur oxides, carbon monoxide, hydrocarbons, and particulate matter. These emissions contribute to climate change and air pollution. Nitrogen oxides, sulfur oxides, and particulate matter pose health risks, while carbon dioxide is a major contributor to global warming. Addressing these emissions is crucial for environmental and public health concerns. [1].

The primary concern in ship emissions is currently carbon dioxide, a significant greenhouse gas. The 21st Conference of the Paris in 2015 aimed to limit the global average temperature increase to below 2°C compared to pre-industrial levels, with an even more ambitious target of 1.5 degrees Celsius. This underlines the critical importance of addressing and reducing carbon dioxide emissions from ships to mitigate the impact of climate change. [2]. The UNFCCC asked the IPCC to release a Special Report on limiting global warming to 1.5 degrees. This request underscores the importance of interdisciplinary research in comprehensively addressing the issues associated with global warming [3]. The agreement mandates countries to voluntarily submit targets for reducing

greenhouse gas emissions, highlighting voluntary efforts beyond the established climate change framework. Consistent with UN recommendations on climate change, regulations on greenhouse gases have also been implemented in the shipping industry. In 2018, greenhouse gas emissions from ships amounted to 1076 million tons, accounting for 2.9% of the total global greenhouse gas emissions [4]. Greenhouse gas emissions from the shipping industry have approximately doubled from 1971 to 2019. Projections from the International Maritime Organization (IMO) indicate that without prompt and robust regulatory interventions, emissions are expected to increase by 90-130% by the year 2050. This underscores the pressing need for effective measures to curb emissions in the maritime sector and mitigate its impact on climate change [5]. Greenhouse gas regulation discussions for ships started at the 23rd General Assembly of the International Maritime Organization in 2003. [6]. At the 62nd MEPC meeting, the IMO adopted an amendment adding MARPOL Annex Chapter VI, mandating the Energy Efficiency Existing Ship Index (EEDI) for all ships and marking a substantial start to greenhouse gas regulation [7]. In April 2018, the IMO adopted the Initial IMO Strategy, aiming to reduce total annual greenhouse gas emissions from shipping by over 50% by 2050 compared to 2008 levels. The strategy emphasizes incremental efforts to achieve this ambitious long-term goal [8]. The Initial IMO Strategy includes an interim target of reducing carbon dioxide emissions per transport operation by at least 40% by 2030. To comply with these reinforced regulations, numerous technologies aimed at reducing greenhouse gas emissions are undergoing development. These technologies can be broadly categorized into those focusing on improving energy efficiency and those involving alternative fuels to achieve carbon reduction [9]. Various energy efficiency improvement technologies, including adjustments to vessel size, hull shape, lightweight materials, air lubrication, hybrid power systems, and waste heat recovery, exhibit the potential to reduce CO2 emissions in the range of 1% to 35%. On the other hand, alternative marine fuels, such as liquefied natural gas, hydrogen, ammonia, methanol, ethanol, biofuels, and electricity, have demonstrated a remarkable potential for emission reduction, reaching up to 80%. These technologies represent promising avenues for achieving substantial reductions in greenhouse gas emissions from the maritime sector [10].

Nitrogen oxide regulations by the International Maritime Organization have undergone incremental strengthening. Compared to the initial regulations implemented in 2000, the second-stage regulations in 2011 were 20% more stringent, and the third-stage regulations in 2016 represented an 80% increase in strength. Additionally, regulations governing sulfur content in marine fuel have also been reinforced, reducing from 4.5% in 2005 to 3.5% in 2012, and further to 0.5% from the year 2020 [11,12]. Sulfur oxide reduction technology has two main approaches: using low-sulfur fuel and employing a sulfur scrubber to remove sulfur oxides from exhaust gas. These methods are relatively simple. Nitrogen oxide reduction methods are divided into in-cylinder technology and after-treatment technology [13]. In-cylinder treatment focuses on lowering the combustion chamber temperature to mitigate the reaction of nitrogen and reduce nitrogen oxide emissions. Technologies for achieving this reduction include introducing moisture into the intake air, utilizing emulsion technology that blends water with fuel, and directly injecting water into the cylinders during the combustion process [14–16], fuel injection system improvement technology [17,18], and exhaust gas recirculation technology [19,20]. The predominant after-treatment technology, Selective Catalytic Reduction (SCR), removes nitrogen oxides by introducing ammonia or urea into the exhaust gas stream [21,22]. Regarding carbon monoxide (CO), hydrocarbons (HC), and particulate matter (PM), which are other exhaust emissions, there are currently no official regulations in place. However, at the 57th meeting of the International Maritime Organization (IMO), the Marine Environment Protection Committee (MEPC) proposed an amended regulation 14 that includes provisions for regulating HC emissions and PM, encompassing ozone-depleting substances. This indicates a potential move towards addressing and regulating these additional pollutants in the future. [23].

Numerous new technologies are under development to comply with the strengthened regulations. However, the technologies actually applied to ships are currently limited and include engine tuning, bulbous bows, pre/post swirl devices, and waste heat recovery. Despite ongoing advancements, the adoption of alternative fuels in the maritime industry remains relatively low [24].

 doi:10.20944/preprints202311.1373.v1

From this perspective, heavy fuel oil (HFO) is expected to persist as the primary fuel for ships. However, there is a concern that the predominant focus on new, zero-carbon fuels might lead to a decline in research dedicated to enhancing the performance and reducing emissions of marine diesel engines, particularly those utilizing HFO. While after-treatment technologies to meet regulations are actively being developed, there is a notable decrease in research on diesel engine combustion. It is crucial to continue studying engine combustion using HFO, which currently dominates the marine fuel landscape. The behavior of fuel spray in the diesel combustion chamber stands out as the most critical factor influencing engine combustion performance. To simultaneously mitigate nitrogen oxides and particulate matter, injection control technology, which reduces the rich mixture area and lowers local combustion temperatures, has been successfully developed for small automobile engines. Applying similar principles to marine diesel engines using HFO could be essential for achieving improved combustion performance and meeting emission reduction targets [25–28]. Research is underway to reduce nitrogen oxide emissions and fuel consumption in marine diesel engines by implementing multiple injection and pre-injection technologies through the common-rail fuel injection system [29]. Moreover, studies have been conducted to enhance the fuel distribution characteristics by improving the shape of the nozzle and the internal hole within the fuel injection valve [30–33]. It appears that research on improving these injection systems is currently limited, with a focus primarily on technologies applicable to new ships.

To meet emission regulations such as nitrogen oxides set by the IMO and the requirements outlined in the IPCC's Special Report on limiting global warming to 1.5 degrees, relying solely on new technologies currently under research may prove challenging. It becomes crucial to continually enhance existing marine diesel engines, particularly those using heavy fuel oil (HFO), which are anticipated to remain in use for the foreseeable future. This study aims to underscore the importance of performance improvement research on existing ship diesel engines and enhance the combustion performance of operational ships. The analysis focuses on combustion characteristics concerning the injection conditions of the fuel injection systems, which can be feasibly improved in the field. The study delves into the effects of fuel injection pressure, injection timing, and spray angle on combustion in a long-stroke cycle marine diesel engine, commonly employed as the main engine in ships. Detailed analyses encompass the behavior of fuel within the combustion chamber, flame temperature, combustion products, and more. The study aims to provide insights into the impact on exhaust emissions, contributing to the overall efficiency enhancement and reduction of exhaust emissions from existing ships. This research aligns with the imperative of continuously improving and optimizing existing technologies for a more sustainable maritime industry.

2. Mathematical Model and Calculation Conditions

The objective of this study is to analyze the combustion behavior within cylinders with the aim of enhancing the performance of existing ship engines. To achieve this, the widely used KIVA code was employed for the combustion calculations of the internal combustion engine. The validation of this code involved comparing combustion, spray, and turbulence models with experimental results, ensuring the accuracy and reliability of the computational simulations used in the study. This approach enables a comprehensive analysis of combustion processes and contributes to improving the understanding and performance of existing ship engines [34–39], and the effect of the grid was also evaluated [40–43]. The combustion behavior was assessed by applying the code to an operating engine. The results were validated, demonstrating consistency with experimental data for parameters such as swirl flow, turbulent flow, spray and combustion characteristics, cylinder pressure, heat release rate, and nitrogen oxides generation. This validation confirms the reliability of the computational simulations using the KIVA code in capturing essential aspects of combustion behavior in ship engines [44–48]. Having been successfully verified, this code has been widely applied in the development and improvement of numerous diesel engines. The validation of the code enhances its credibility and applicability [49–54].

Preprints (www.preprints.org) | NOT PEER-REVIEWED | Posted: 22 November 2023 doi:10.20944/preprints202311.1373.v1

2.1. Mathematical Model

The computational program used to analyze the combustion behavior is KIVA and the transport equations are given as follows [55].

The continuity equation for species m is

$$\frac{\partial \rho_m}{\partial t} + \nabla\cdot(\rho_m u) = \nabla\cdot[\varrho D \nabla(\frac{\rho_m}{\rho})] + \dot{\rho}_m^c + \dot{\rho}^s \delta_{m1} \quad (1)$$

where ρ_m is the mass density of species m, ρ is the total mass density, and u is the fluid velocity. D is the diffusion coefficient and source terms given by the chemical reaction $\dot{\rho}_m^c$ and the droplet evaporation $\dot{\rho}^s$, and δ is Dirac delta function.

The total fluid continuity equation summing Eq.(1) over all species is

$$\frac{\partial \rho}{\partial t} + \nabla\cdot(\rho u) = \dot{\rho}^s \quad (2)$$

Since mass is conserved in chemical reactions.

The momentum is

$$\frac{\partial(\rho u)}{\partial t} + \nabla\cdot(\rho u u) = -\frac{1}{a^2}\nabla p - A_o \nabla 2/3 \varrho k + \nabla\cdot\sigma + F^s + \rho g \quad (3)$$

where p is the fluid pressure. The dimensionless quantity α is used in conjunction with the pressure gradient scaling method. The quantity A_o is unity in the turbulence calculation.

The viscous stress tensor is

$$\sigma = \mu[\nabla u + (\nabla u)^T] + \lambda\, \nabla\cdot u\, I \quad (4)$$

where μ and λ are the first and second coefficients of viscosity. The superscript T denotes the transpose and I is the unit dyadic.

The internal energy equation is

$$\frac{\partial(\rho I)}{\partial t} + \nabla\cdot(\rho u I) = -\rho\, \nabla\cdot u + (I - A_o)\sigma : \nabla u - \nabla\cdot J + A_o \rho\varepsilon + \dot{Q}^c + \dot{Q}^s \quad (5)$$

where I is the specific internal energy, exclusive of chemical energy. The heat flux vector J is the sum of contributions due to heat conduction and enthalpy diffusion:

$$J = -K\nabla T - \rho D \sum_m h_m \nabla\left(\frac{\rho_m}{\rho}\right) \quad (6)$$

where T is the fluid temperature and h_m is the specific enthalpy of species m. $\dot{Q}^c$ and $\dot{Q}^s$ are the chemical heat release and spray interactions.

Two transport equations are solved for the turbulent kinetic energy and its dissipation rate.

$$\frac{\partial(\rho k)}{\partial t} + \nabla\cdot(\rho u k) = -\frac{2}{3}\rho\, k \nabla\cdot u + \sigma : \nabla u + \nabla\cdot[(\frac{\mu}{p_{r_k}})\nabla k] - \rho\varepsilon + \dot{W}^s \quad (7)$$

And

$$\frac{\partial(\rho\varepsilon)}{\partial t} + \nabla\cdot(\rho u \varepsilon) = -\left(\frac{2}{3}c_{\varepsilon_1} - c_{\varepsilon_3}\right)\rho\, \varepsilon \nabla\cdot u + \nabla\cdot[(\frac{\mu}{p_{r_\varepsilon}})\nabla\epsilon] + \frac{\varepsilon}{k}\left[c_{\varepsilon_1}\sigma : \nabla u - c_{\varepsilon_2}\rho\varepsilon + c_s \dot{W}^s\right] \quad (8)$$

The source term $-\left(\frac{2}{3}c_{\varepsilon_1} - c_{\varepsilon_3}\right)\rho\, \varepsilon \nabla\cdot u$ in the e-equation accounts for length scale changes when there is velocity dilatation. Source terms involving the quantity $\dot{W}^s$ arise due to interaction with the spray. The quantities c_{ε_1}, c_{ε_1}, c_{ε_1}, p_{r_ε} and p_{r_c} are constants, and their values are determined through experiments and theoretical considerations.

Preprints (www.preprints.org) | NOT PEER-REVIEWED | Posted: 22 November 2023 doi:10.20944/preprints202311.1373.v1

2.2. Calculation Conditions and Grids

Figure 1 shows the mesh shape at crank angles of 0 degrees, 30 degrees, and 90 degrees. The mesh was generated by inputting the shape of the piston crown and head of the target engine. An automated mesh generator integrated into the internal combustion analysis code was employed to create this mesh.

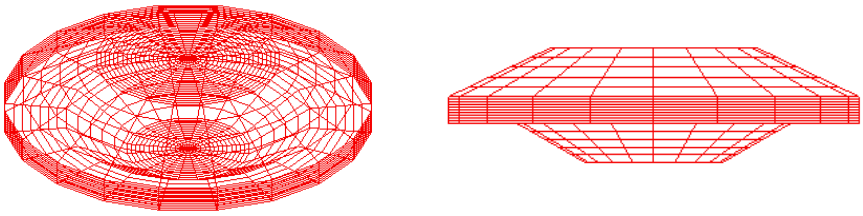

(**a**) At TDC

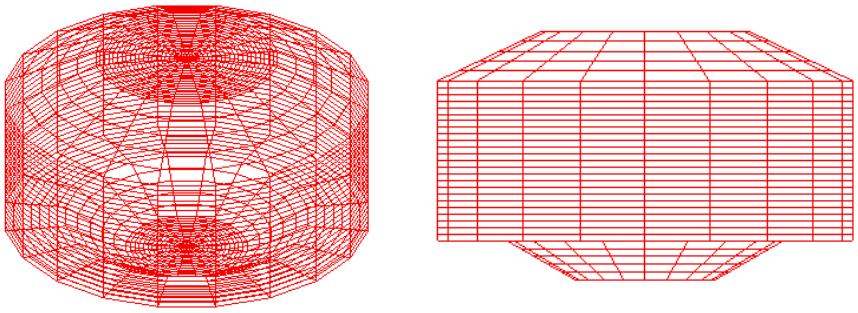

(**b**) At 30 CA

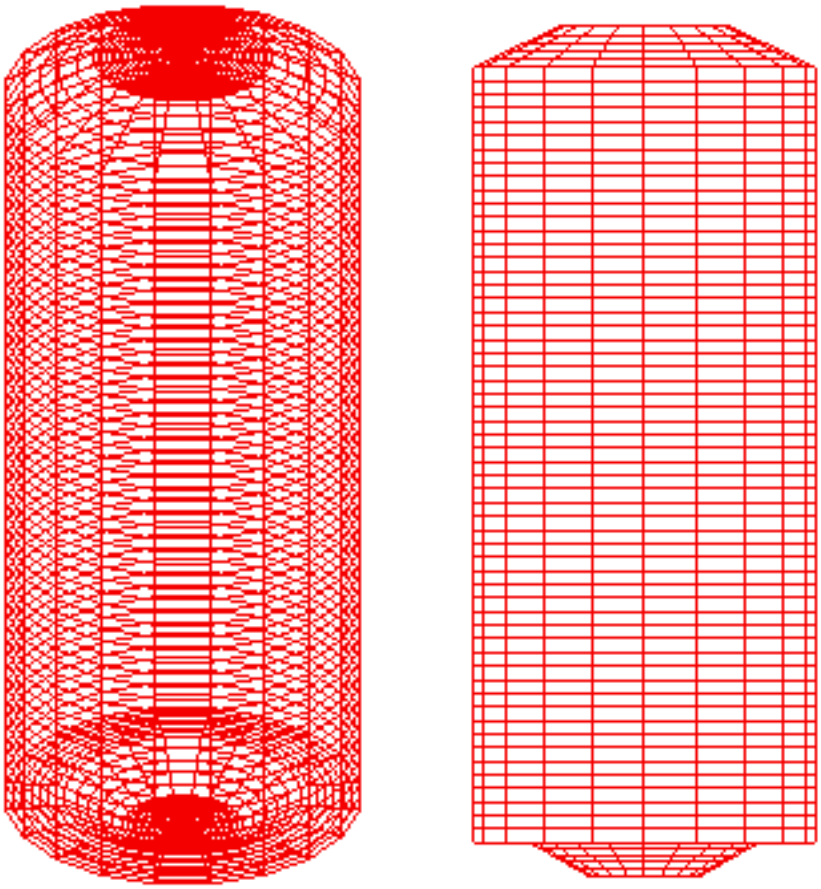

(**c**) At 90 CA

Figure 1. Calculation grids according to crank angle.

Preprints (www.preprints.org) | NOT PEER-REVIEWED | Posted: 22 November 2023 doi:10.20944/preprints202311.1373.v1

Table 1 presents the engine specifications and calculation conditions. The target engine is commonly utilized in existing ships and is characterized as a long-stroke engine with a stroke-to-bore ratio of 3.2. The engine load chosen corresponds to 70% of the maximum cruising rate, which is the typical operating speed for ships. The specified operating output is 500 kW per cylinder, with a fuel injection mass of 8 grams per stroke. In this study, the calculation conditions were chosen to represent changeable field conditions for improving the targeted marine engine. The injection pressure used in the calculations is categorized into 5 stages, ranging from 20 MPa to 160 MPa. Injection timing varies from BTDC 15 to ATDC 5 degrees, and the spray angle is adjusted from 10 degrees to 50 degrees at 10-degree intervals. Additional details are provided in the table.

Table 1. Engine specification and calculation conditions.

Cases	Variable	
Target engine & base conditions	Type of target engine	2-stroke cycle
	Operating output(kW/cyl)	500
	Engine speed(rpm)	180
	BorexStroke(cm)	42x136
	Crank angle at compression start(CA)	ATDC 120
	Crank angle at exhaust valve open(CA)	BTDC 120
	Number of nozzle hole(EA)	1
	Mass flow of fuel injection per stroke(g/stroke)	8
	Fuel injection pressure(MPa)	40
	Fuel spray angle(deg)	30
	Injection duration(CA)	10
	Wall temperature(°C)	150
	Initial air temperature(°C)	60
	Initial air pressure(MPa)	0.15
	Length of connecting rod(cm)	182
	Compression ratio	28.6
Injection pressure variation	Fuel injection pressure(MPa)	20 40 80 120 160
Injection timing variation	Injection timing(CA)	BTDC 15 BTDC 10 BTDC 5 TDC ATDC 5
Spray angle variation	Spray angle(Deg)	10 20 30 40 50

3. Results

3.1. Injection Pressure Variaion

Figures 2–4 show the fuel distribution in the combustion chamber, the fuel mass, and the remaining fuel amount at ATDC 120 when the exhaust valve is opened. The fuel injection period spans from 10 degrees before top dead center to top dead center. During this interval, both fuel supply through injection and fuel consumption due to combustion concurrently influence the distribution of fuel within the combustion chamber. At a low injection pressure of 20 MPa, the fuel distribution exhibits a high concentration, forming in a narrow area from the injection valve to the center of the cylinder. This concentration is attributed to the slower propagation of fuel under lower injection pressures. From top dead center (TDC) to after top dead center (ATDC) 30, a considerable

Preprints (www.preprints.org) | NOT PEER-REVIEWED | Posted: 22 November 2023 doi:10.20944/preprints202311.1373.v1

amount of the fuel that descends along the piston is dispersed over the upper surface of the piston. With an increase in injection pressure, the high-concentration fuel distribution area undergoes a rapid reduction. At an injection pressure of 80 MPa or higher, this high-concentration fuel region disappears entirely by after top dead center (ATDC) 10. Conversely, when the injection pressure is low, a substantial amount of fuel is observed to be distributed to the piston crown at ATDC 120 when the exhaust valve is opened.

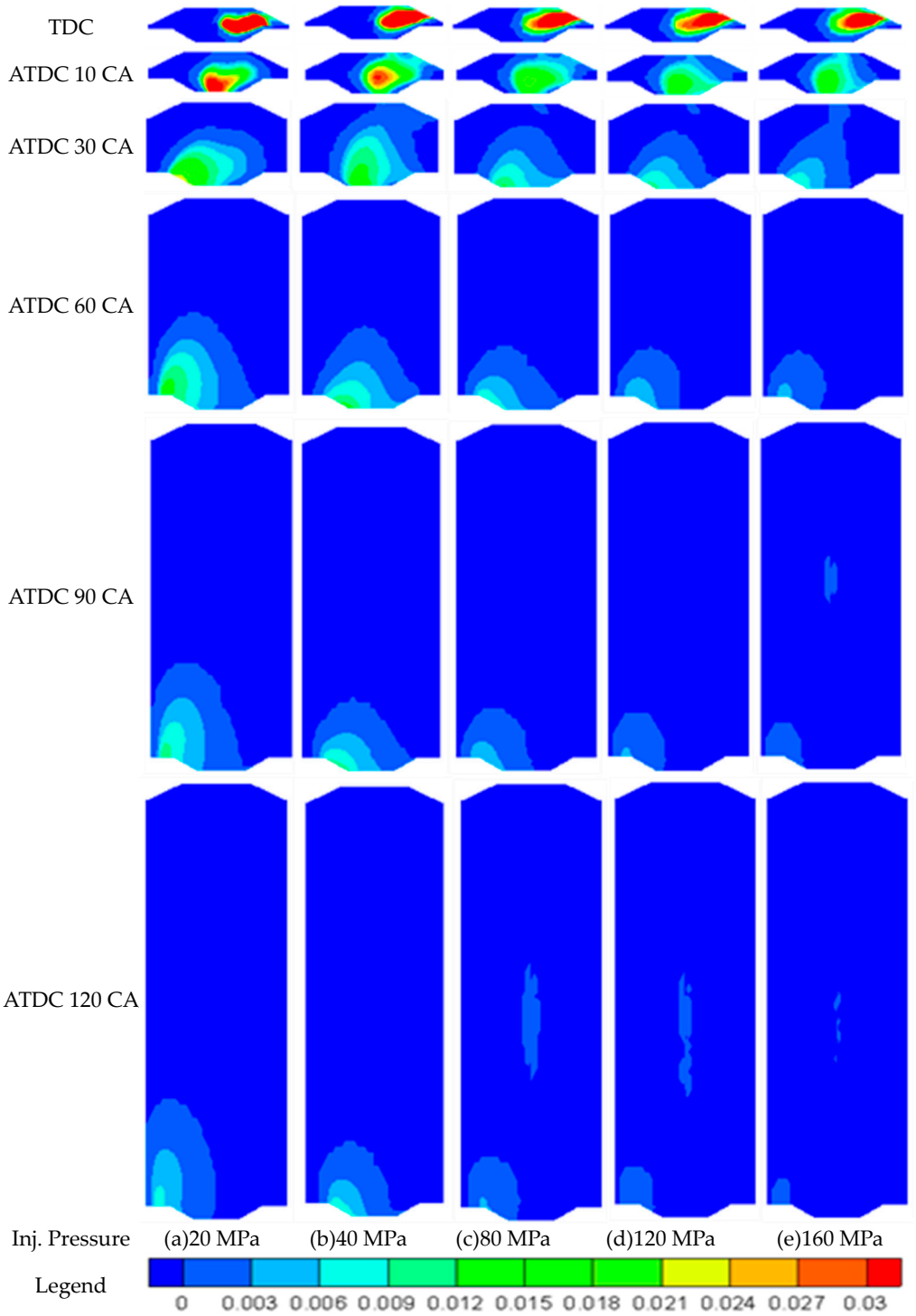

Figure 2. Fuel volume fraction distribution at the center section of combustion chamber.

Preprints (www.preprints.org) | NOT PEER-REVIEWED | Posted: 22 November 2023 doi:10.20944/preprints202311.1373.v1

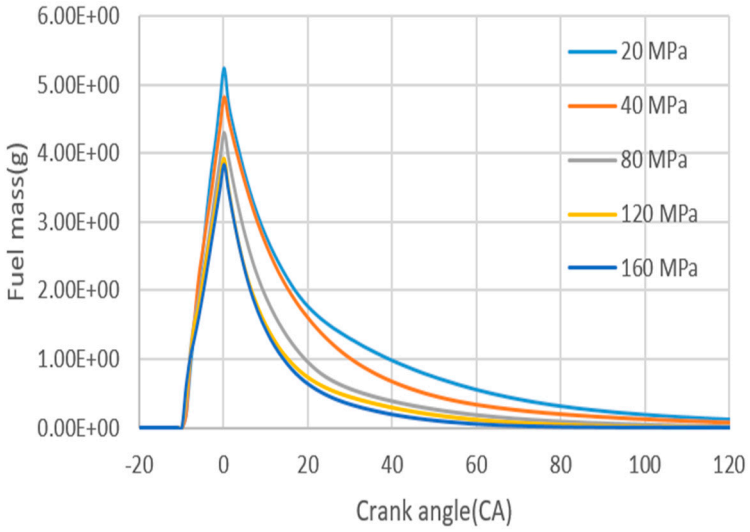

Figure 3. Residual fuel mass with injection pressure variation.

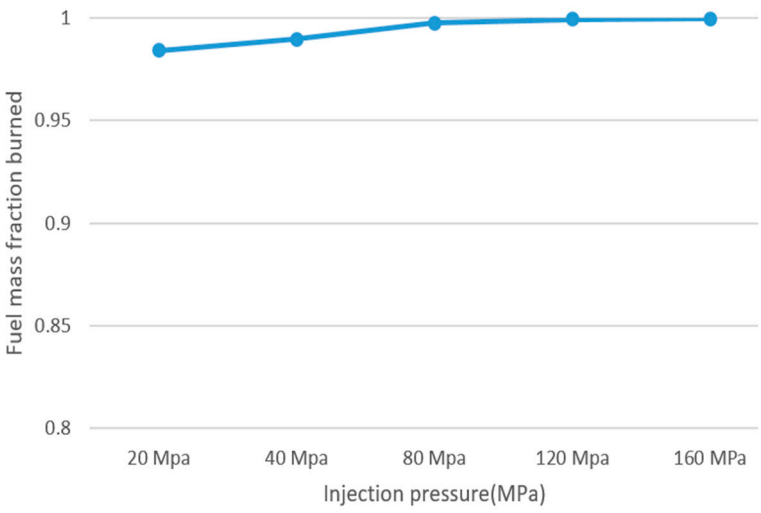

Figure 4. Fuel mass fraction burned at the exhaust valve open with injection pressure variation.

During the period from before top dead center (BTDC) 10 to top dead center (TDC) during fuel injection, the injected fuel propagates into the cylinder. The fuel undergoes evaporation while being mixed with the surrounding air, and combustion progresses. In the case of a low injection pressure of 20 MPa, 34% of the fuel is consumed at TDC, while in the case of 160 MPa, 53% of the fuel is consumed. By after top dead center (ATDC) 30, 83% of the fuel is burned at low pressure, increasing to 95% with higher injection pressure. The amount of fuel burned at the time the exhaust valve is opened is also nearly 100%, particularly in the case of high injection pressure.

Figure 5 shows the temperature distribution in the cylinder, spanning from the piston at top dead center to a crank angle of 120 degrees when the exhaust valve opens. At low injection pressures (below 40 MPa), a locally formed high-temperature region with a robust combustion rate emerges at the top of the cylinder. This region gradually expands, persisting with a significant temperature presence until the initiation of the exhaust phase. Conversely, when the injection pressure exceeds 80 MPa, the high-temperature region experiences a substantial increase, peaking around After Top Dead Center (ATDC) 10, and it disappears entirely during the exhaust phase.

Preprints (www.preprints.org) | NOT PEER-REVIEWED | Posted: 22 November 2023 doi:10.20944/preprints202311.1373.v1

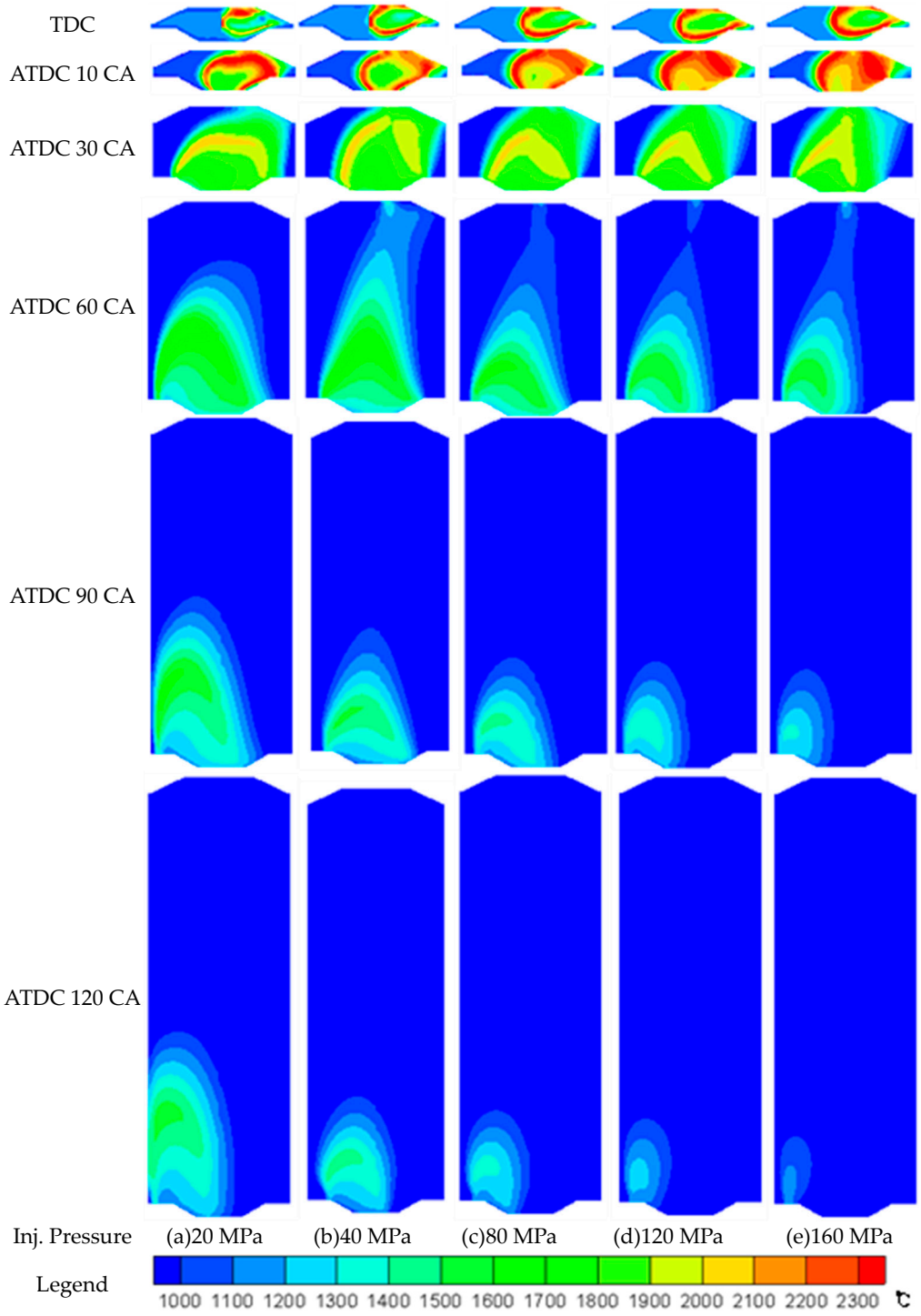

Figure 5. Temperature distribution at the center section of combustion chamber.

The combustion chamber temperature distribution behavior indicates the formation and characteristics of the flame. With low-pressure injection below 40 MPa, combustion occurs slowly, leading to a gradual flame propagation until emission begins. On the other hand, higher injection pressures cause an immediate widening of the high-temperature region after injection, resulting in a more active and rapid combustion process.

Figure 6 displays changes in cylinder pressure as injection pressure rises from 20 MPa to 160 MPa. The peak cylinder pressure, occurring just after Top Dead Center (TDC), shows a 7.7% increase with higher injection pressure. This aligns with the observed trend of a substantial increase in the combustion progress rate with elevated injection pressure.

Preprints (www.preprints.org) | NOT PEER-REVIEWED | Posted: 22 November 2023 doi:10.20944/preprints202311.1373.v1

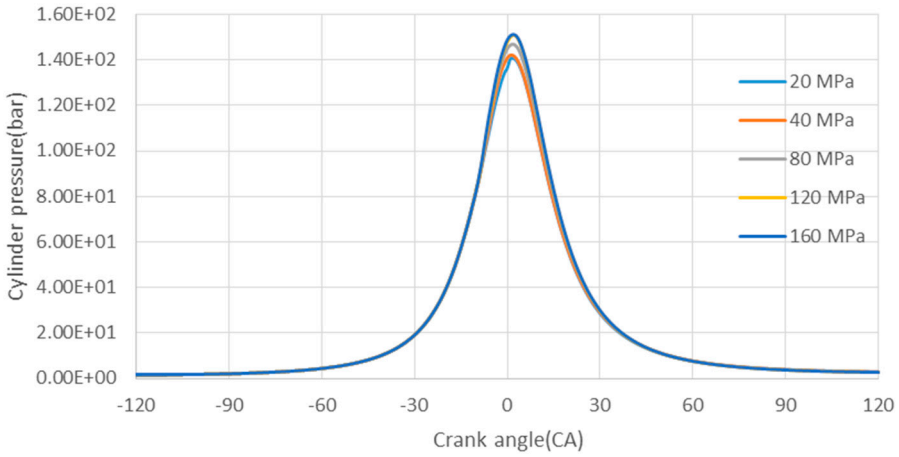

Figure 6. Cylinder pressure variation with fuel injection pressures.

Figure 7 shows the distribution of OH radicals, crucial intermediate products in combustion. The behavior of OH, representing the flame front, is vital for understanding flame propagation. OH has the widest distribution at After Top Dead Center (ATDC) 10. At low injection pressures, OH is concentrated near the injection valve, but at high pressures, it is distributed extensively, indicating an increased flame surface and combustion rate. After ATDC 30, high-pressure injection (over 80 MPa) rapidly decreases OH distribution, while low-pressure injection maintains it.

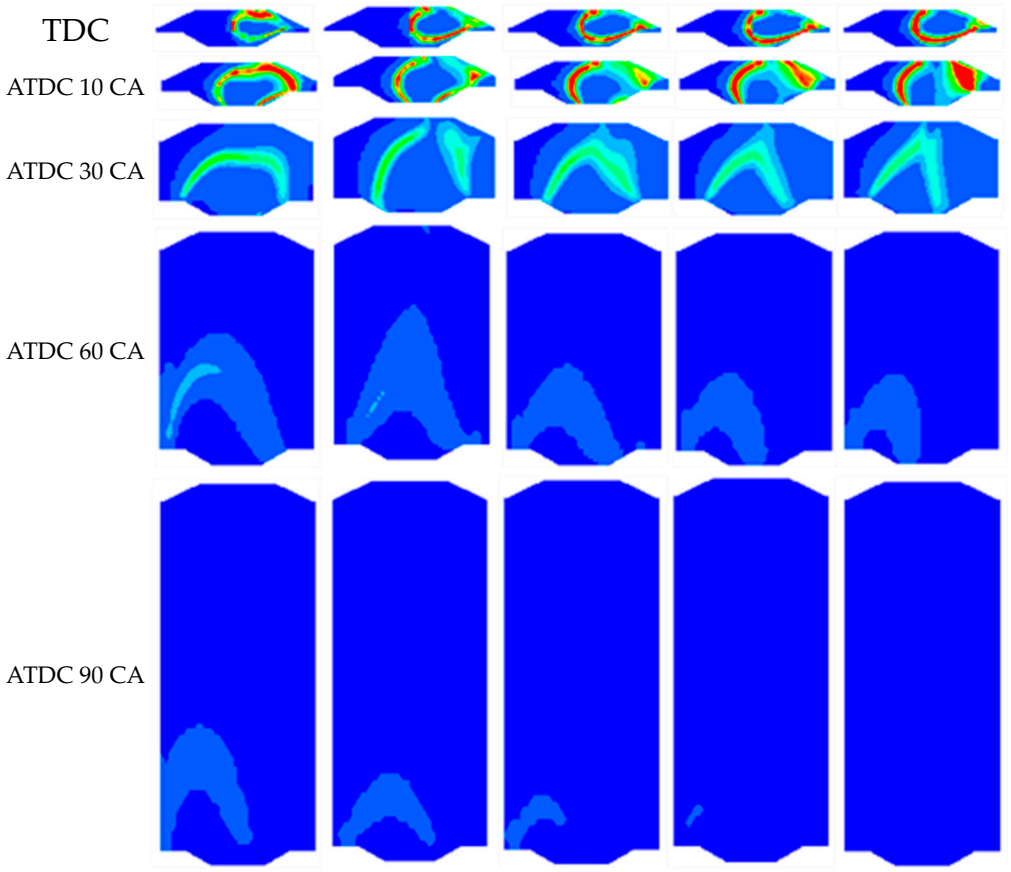

Preprints (www.preprints.org) | NOT PEER-REVIEWED | Posted: 22 November 2023 doi:10.20944/preprints202311.1373.v1

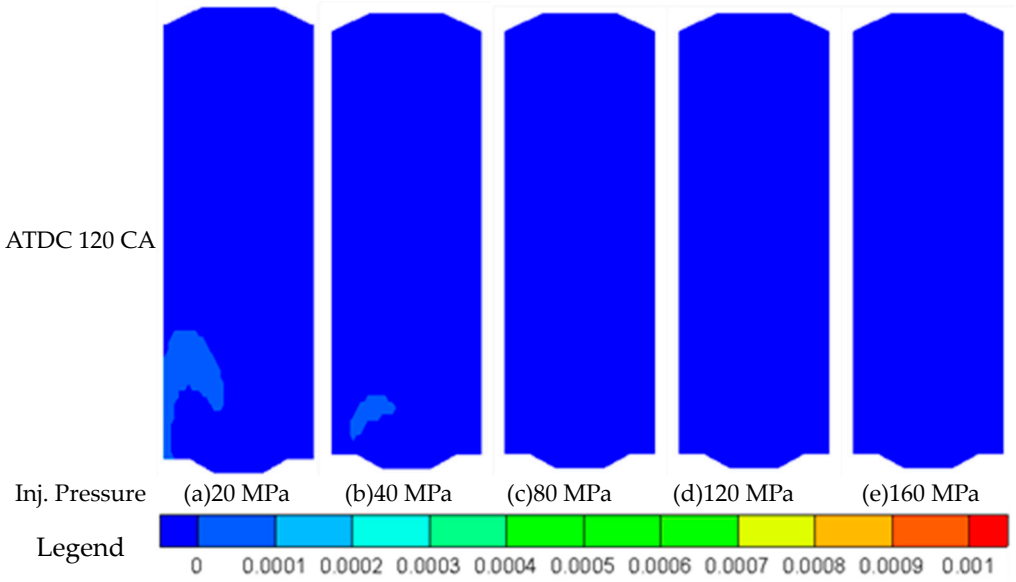

Figure 7. OH radical distribution at the center section of combustion chamber.

Figures 8 and 9 depict the total OH volume fraction in the cylinder across crank angles and at the exhaust valve opening. Near Top Dead Center (TDC), high-pressure injection shows double the OH fraction of low-pressure injection. However, after ATDC 30, high-pressure injection exhibits a lower value. This suggests that in high-pressure injection, rapid combustion occurs immediately after injection, completing by ATDC 30. In low-pressure injection, OH persists at the exhaust valve opening, indicating ongoing combustion and the discharge of unburned fuel.

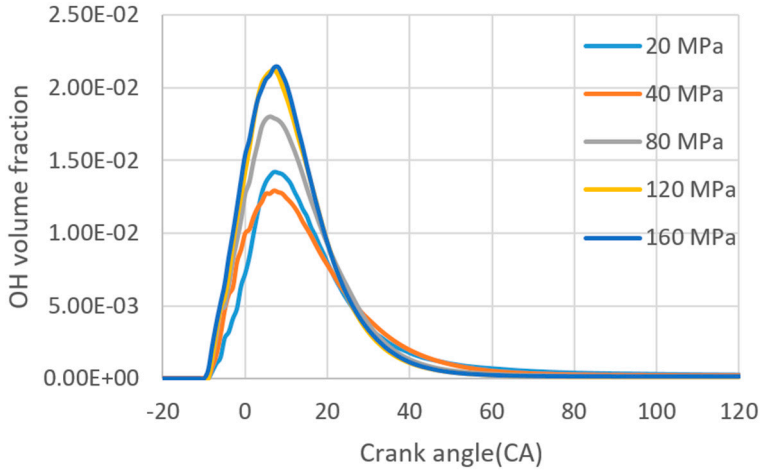

Figure 8. OH radical volume fraction with injection pressure variation.

Preprints (www.preprints.org) | NOT PEER-REVIEWED | Posted: 22 November 2023 doi:10.20944/preprints202311.1373.v1

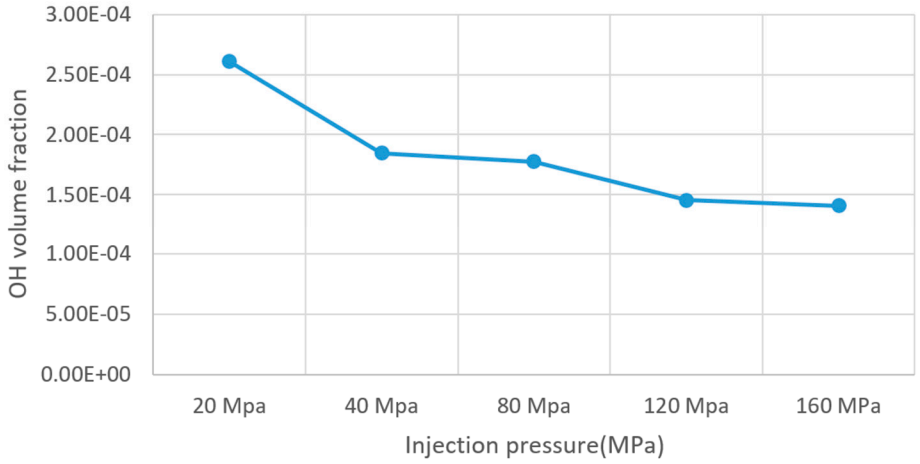

Figure 9. OH radical volume fraction at the exhaust valve open with injection pressure variation.

Figures 10–12 show the distribution of carbon monoxide (CO), the cylinder volume fraction across crank angles, and the volume fraction at exhaust time, respectively. CO is a chemical species generated at the start of combustion and diminishes as combustion progresses, providing insights into the combustion chamber conditions affecting complete combustion. At top dead center, where fuel injection concludes, CO concentration is high around the flame front and decreases behind the flame. With low injection pressure, high concentration is locally observed only around the flame surface. In contrast, high-pressure injection results in a more widely distributed high concentration over the entire flame surface. At ATDC 10, this phenomenon intensifies, and in high-pressure injection (over 120 MPa), high-concentration CO spreads to occupy the entire cylinder center. Conversely, after ATDC 30, lower injection pressure exhibits a broader CO distribution, persisting until exhaust. Similar to concentration distribution, the CO volume fraction for the entire cylinder peaks around Before Top Dead Center (BTDC) 10 and then rapidly decreases. The maximum CO concentration increases by over 50% at injection pressures exceeding 120 MPa and decreases by over 99% at exhaust valve opening. This suggests that in low-pressure injection, the fuel does not propagate far, forming a high-concentration area and resulting in slow combustion. In high-pressure injection, the fuel propagates rapidly over a wide area, leading to rapid combustion.

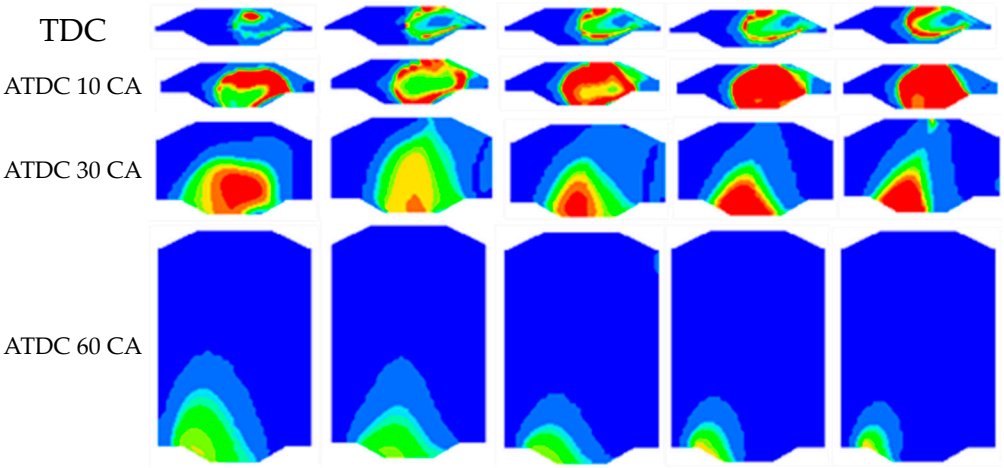

Preprints (www.preprints.org) | NOT PEER-REVIEWED | Posted: 22 November 2023 doi:10.20944/preprints202311.1373.v1

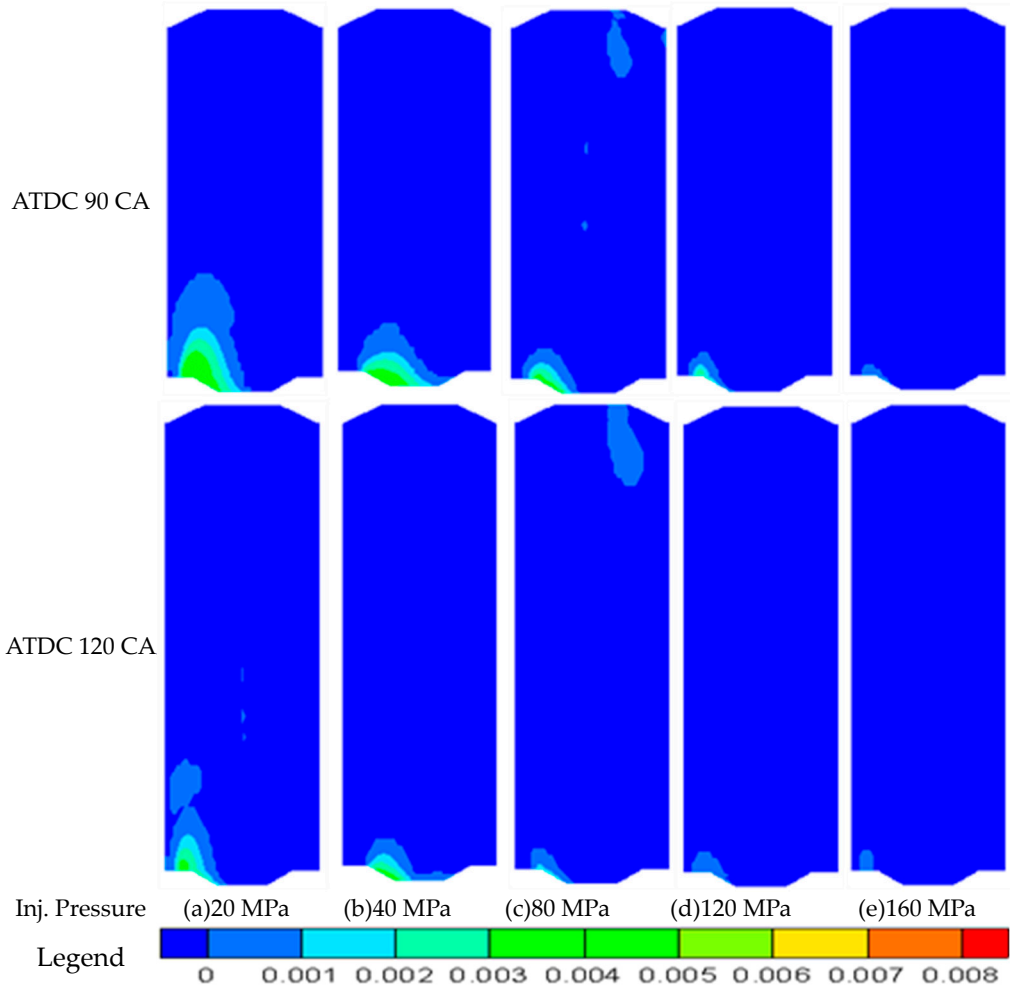

Figure 10. CO distribution at the center section of combustion chamber.

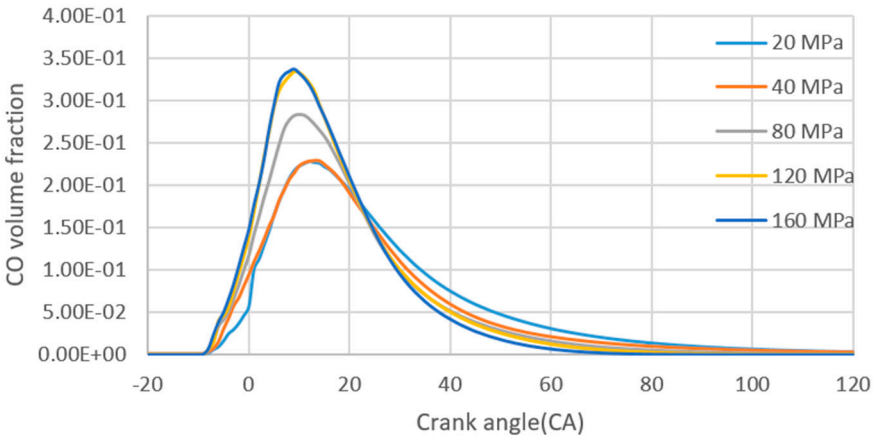

Figure 11. CO volume fraction with injection pressure variation.

Preprints (www.preprints.org) | NOT PEER-REVIEWED | Posted: 22 November 2023 doi:10.20944/preprints202311.1373.v1

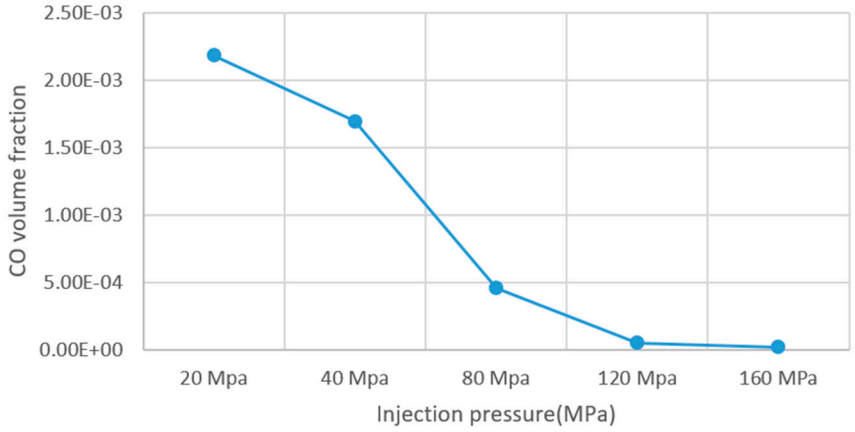

Figure 12. CO volume fraction at the exhaust valve open with injection pressure variation.

Figures 13–15 show the distribution of nitrogen monoxide (NO), the cylinder volume fraction across crank angles, and the volume fraction at exhaust time, respectively. Nitrogen oxides are primarily produced in the high-temperature zone behind the flame, freeze quickly upon production, and persist in that state. In low-pressure injection below 40 MPa, high-concentration nitrogen oxides are narrowly distributed at the top of the cylinder and near the injection valve at Top Dead Center (TDC). Conversely, in high-pressure injection exceeding 120 MPa, high-concentration nitrogen oxides are distributed widely throughout the flame behind. The nitrogen oxide volume fraction for the entire cylinder is predominantly generated up to Before Top Dead Center (BTDC) 10 and maintains a similar value until the exhaust valve opens. The nitrogen oxide concentration at exhaust time increases by over 70% with injection pressure exceeding 120 MPa. This indicates that high-pressure injection leads to a broader distribution of high-concentration nitrogen oxides throughout the flame, contributing to increased nitrogen oxide concentrations at the time of exhaust.

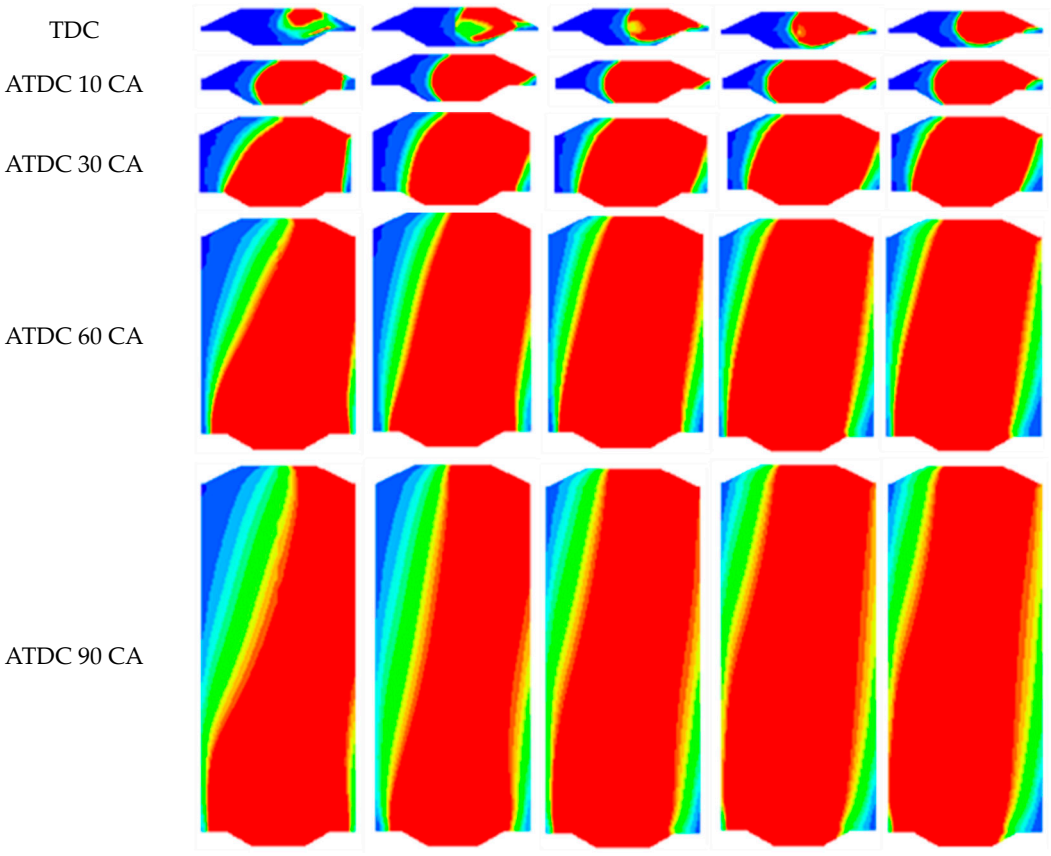

Preprints (www.preprints.org) | NOT PEER-REVIEWED | Posted: 22 November 2023 doi:10.20944/preprints202311.1373.v1

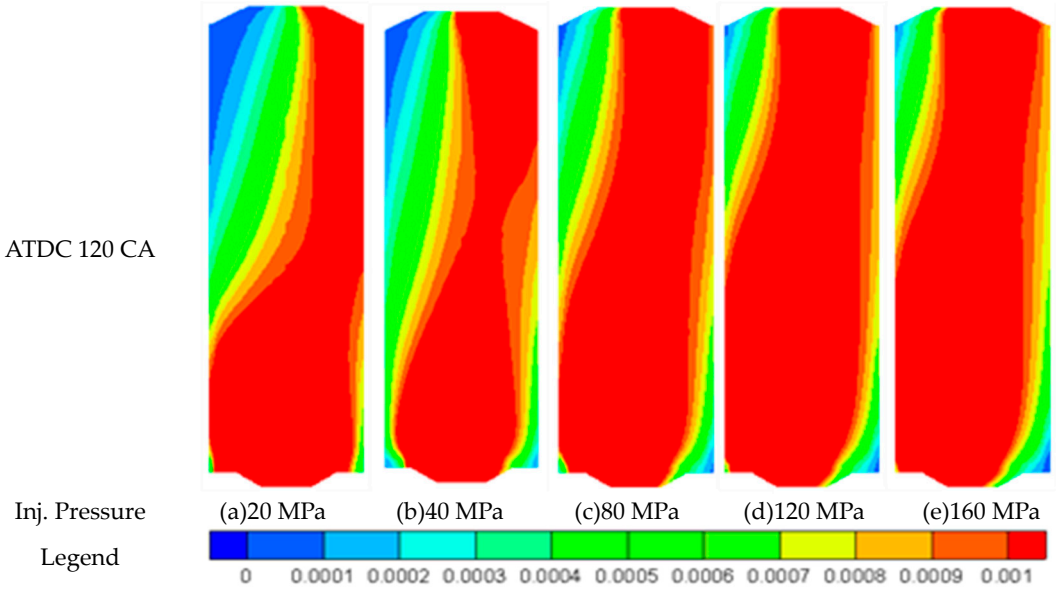

Figure 13. NO distribution at the center section of combustion chamber.

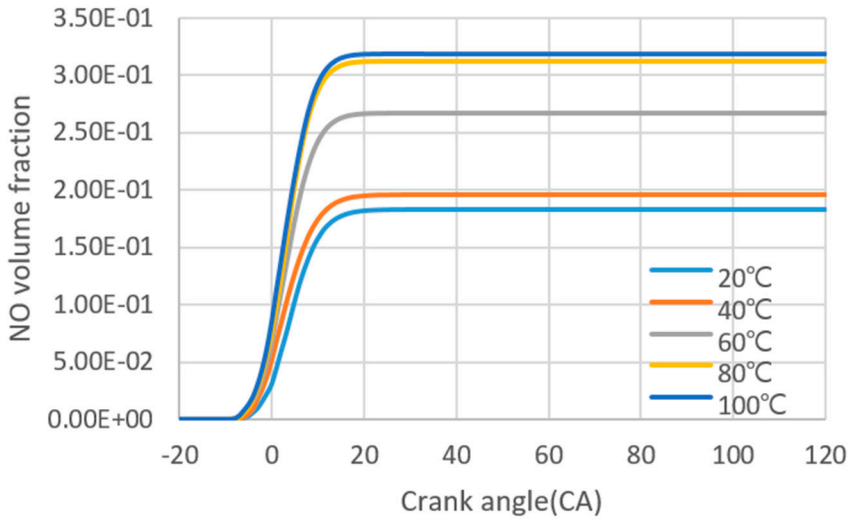

Figure 14. NO volume fraction with injection pressure variation.

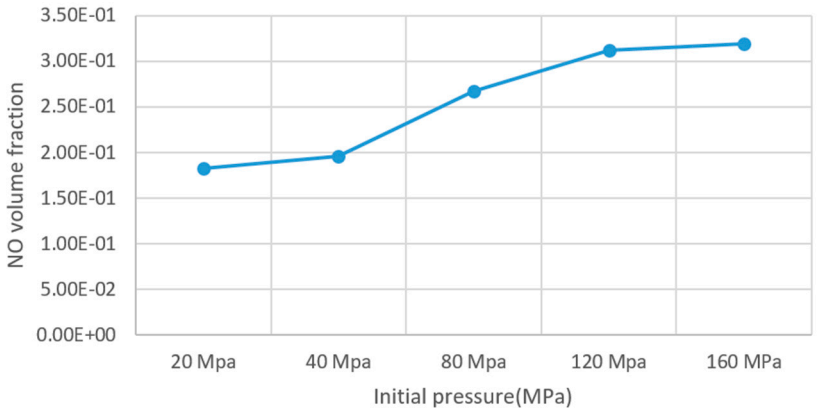

Figure 15. NO volume fraction at the exhaust valve open with injection pressure variation.

Preprints (www.preprints.org) | NOT PEER-REVIEWED | Posted: 22 November 2023 doi:10.20944/preprints202311.1373.v1

3.2. Injection Timing Variaion

In Figure 16, the fuel distribution across the crank angle is shown when the injection timing changes from Before Top Dead Center (BTDC) 15 to After Top Dead Center (ATDC) 5 degrees. If fuel injection starts before BTDC 10, the fuel is concentrated on the piston crown as the piston rises to Top Dead Center (TDC), injected into the combustion chamber in a confined space. However, the combustion rate is slow due to the very cold temperature of the piston walls compared to the flame temperature. When the injection timing is set at BTDC 15, significant combustion occurs during the high-temperature compression process, leading to the burning of most of the fuel despite the slow combustion of the cold piston crown. However, with the injection timing at BTDC 10, a considerable amount of fuel concentrated on the upper wall of the piston remains unburned. This is attributed to the rapid temperature drop as the piston descends, hindering complete combustion.

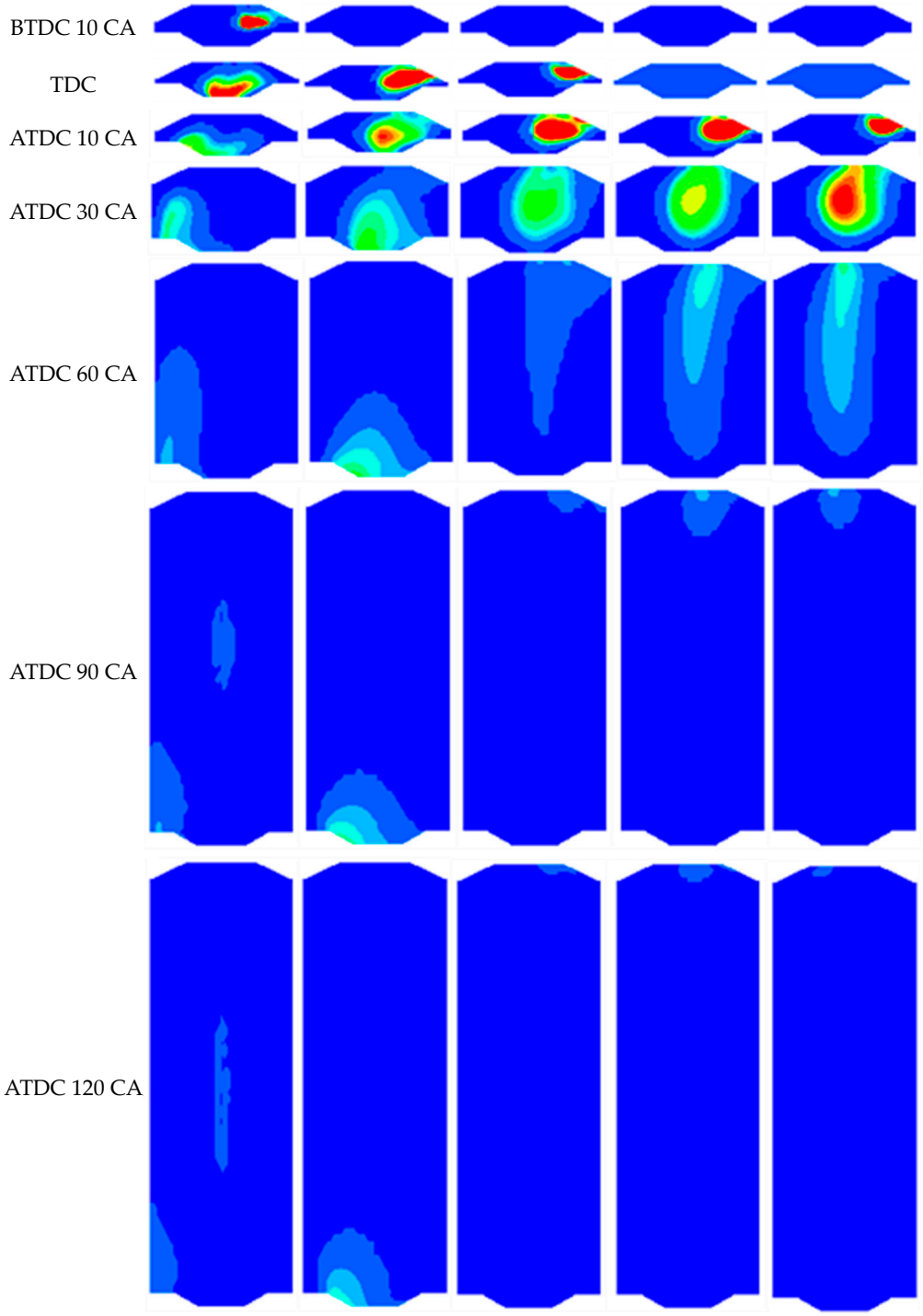

Preprints (www.preprints.org) | NOT PEER-REVIEWED | Posted: 22 November 2023 doi:10.20944/preprints202311.1373.v1

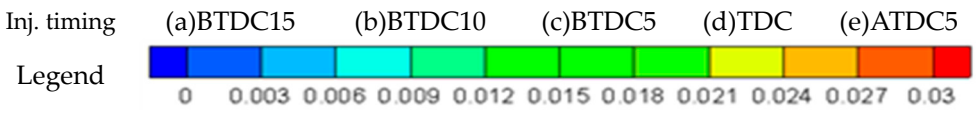

Figure 16. Fuel volume fraction distribution at the center section of combustion chamber.

When the injection timing is set after Before Top Dead Center (BTDC) 5, the expanding space as the piston descends prevents the injected fuel from reaching the piston head surface. As a result, most of the fuel is widely distributed in the inner space of the cylinder. Despite the slow combustion caused by the low temperature, combustion is completed by the time the exhaust valve opens. Figure 17 shows the fuel mass fraction across the crank angle, and Figure 18 shows the mass fraction at the start of exhaust. When the injection timing is delayed, a substantial amount of fuel exists due to slow combustion at the beginning of the combustion process. However, the amount of fuel rapidly decreases afterward due to the onset of rapid combustion. This indicates that a delayed injection timing results in a larger initial quantity of fuel, leading to a slower combustion process initially, followed by a rapid decrease in fuel mass due to accelerated combustion.

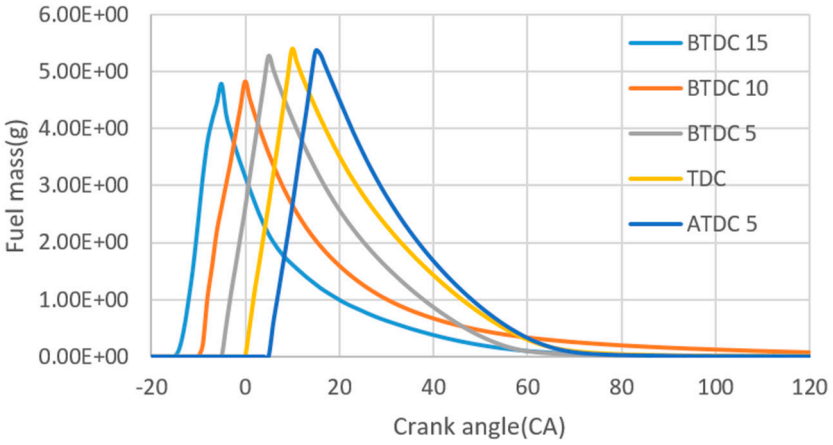

Figure 17. Residual fuel mass with injection timing variation.

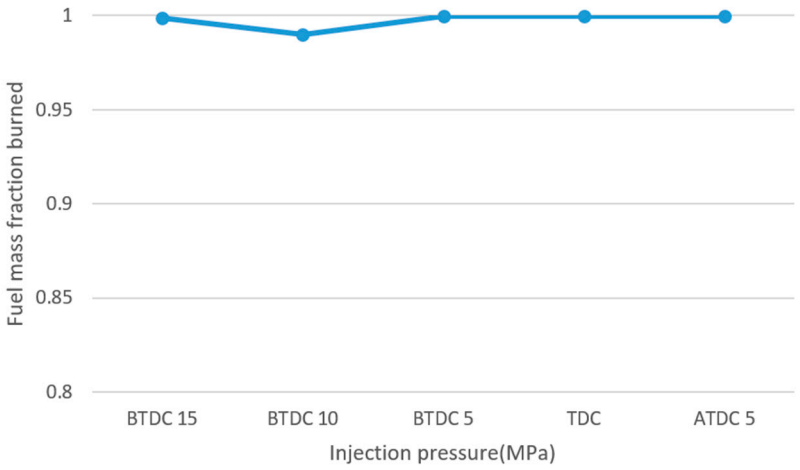

Figure 18. Fuel mass fraction burned at the exhaust valve open with injection timing variation.

Figure 19 shows the temperature distribution in the combustion chamber as the injection timing varies. When the injection starts at Before Top Dead Center (BTDC) 15, fuel is injected during the period when the piston rises, and the injection ends at BTDC 5. When the injection starts at Before Top Dead Center (BTDC) 15, during the piston's ascent to top dead center, the injected fuel descends

 doi:10.20944/preprints202311.1373.v1

to the piston crown and undergoes combustion, resulting in a widely distributed high-temperature area around the piston crown. The most active combustion occurs from Top Dead Center (TDC) to After Top Dead Center (ATDC) 10. Subsequent combustion takes place between the left side of the cylinder and the piston. If injection starts at BTDC 10 and ends at TDC, a high-temperature flame area is distributed around the piston head, resembling the scenario where injection starts at BTDC 15. However, by the time the exhaust valve opens, the high-temperature distribution around the piston crown indicates incomplete combustion with remaining fuel. If the fuel injection timing is after BTDC 5, the injected fuel does not reach the piston crown during the descending piston, and most combustion occurs in the inner space of the cylinder. As the piston moves down, the combustion rate slows due to decreasing temperature and pressure in the combustion chamber. Nevertheless, most of the combustion is completed at the time of exhaust by forming a wide flame area over the entire cylinder.

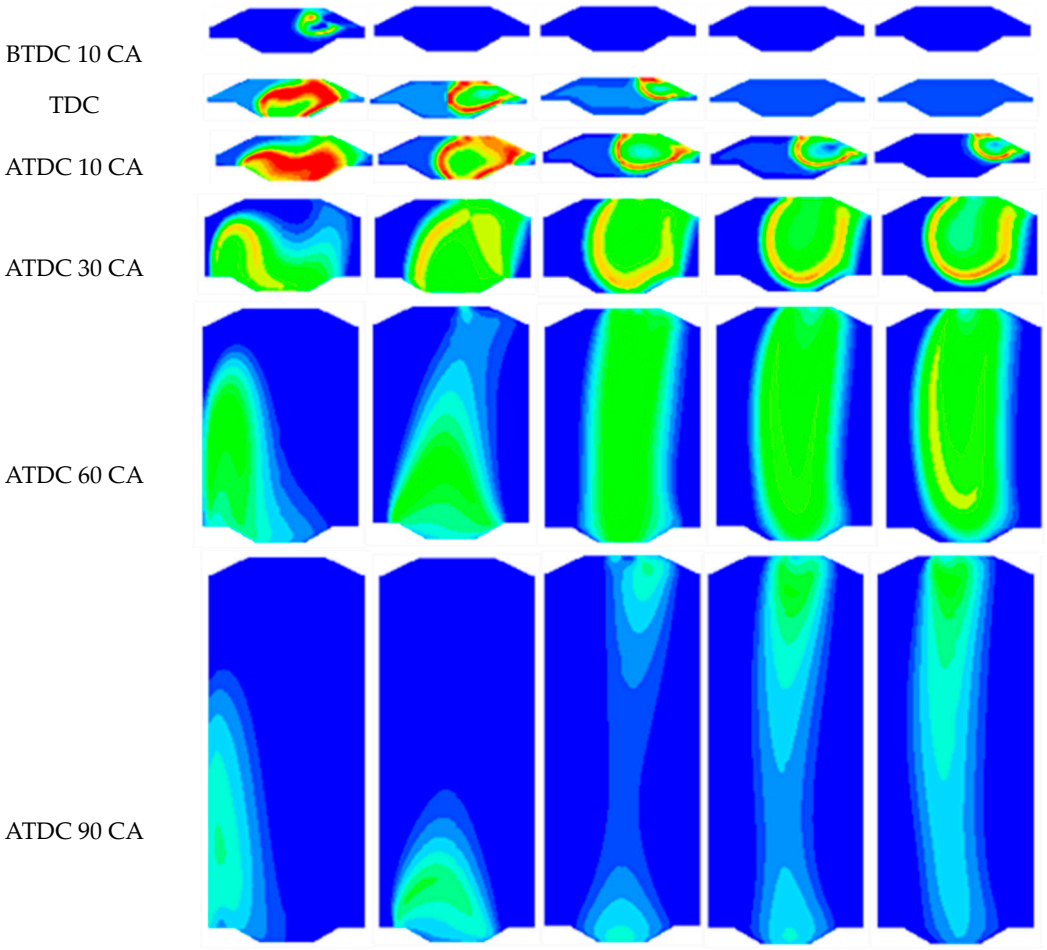

Preprints (www.preprints.org) | NOT PEER-REVIEWED | Posted: 22 November 2023 doi:10.20944/preprints202311.1373.v1

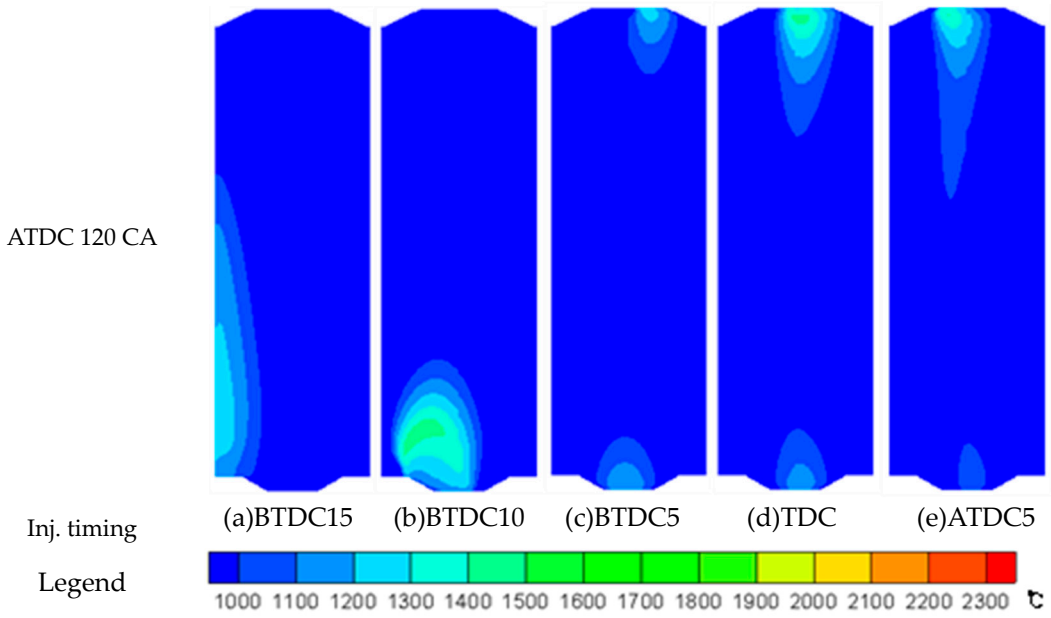

Figure 19. Temperature distribution at the center section of combustion chamber.

Cylinder pressure exhibits significant variation depending on the injection timing. When the injection timing is delayed from Before Top Dead Center (BTDC) 15 to After Top Dead Center (ATDC) 5, the combustion speed at the beginning of injection slows down. As a result, the maximum cylinder pressure decreases from 158 MPa to 120 MPa, as shown in Figure 20.

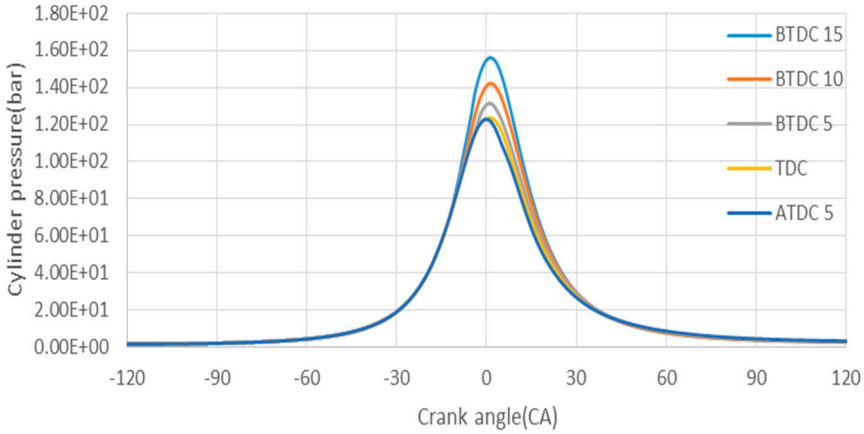

Figure 20. Cylinder pressure variation with fuel injection timing.

In Figure 21, the distribution of the volume fraction of OH radicals, representing the combustion state of the flame front, is illustrated. Observations at different injection timings reveal the following trends. At the injection timing of Before Top Dead Center (BTDC) 15, there is a high-concentration OH volume fraction distributed around the flame surface. This concentration rapidly decreases as the injection timing is delayed. When fuel injection starts after BTDC 5, the high-concentration area completely disappears. Advancing the injection timing results in main combustion occurring while the piston rises, maintaining high temperature and high pressure. This leads to very rapid combustion. Conversely, when the injection timing is delayed, the combustion area widens along the expanding combustion chamber as the piston descends. This expansion, coupled with the effect of lowering ambient temperature, causes a distribution of low-concentration OH over a wide area.

Preprints (www.preprints.org) | NOT PEER-REVIEWED | Posted: 22 November 2023 doi:10.20944/preprints202311.1373.v1

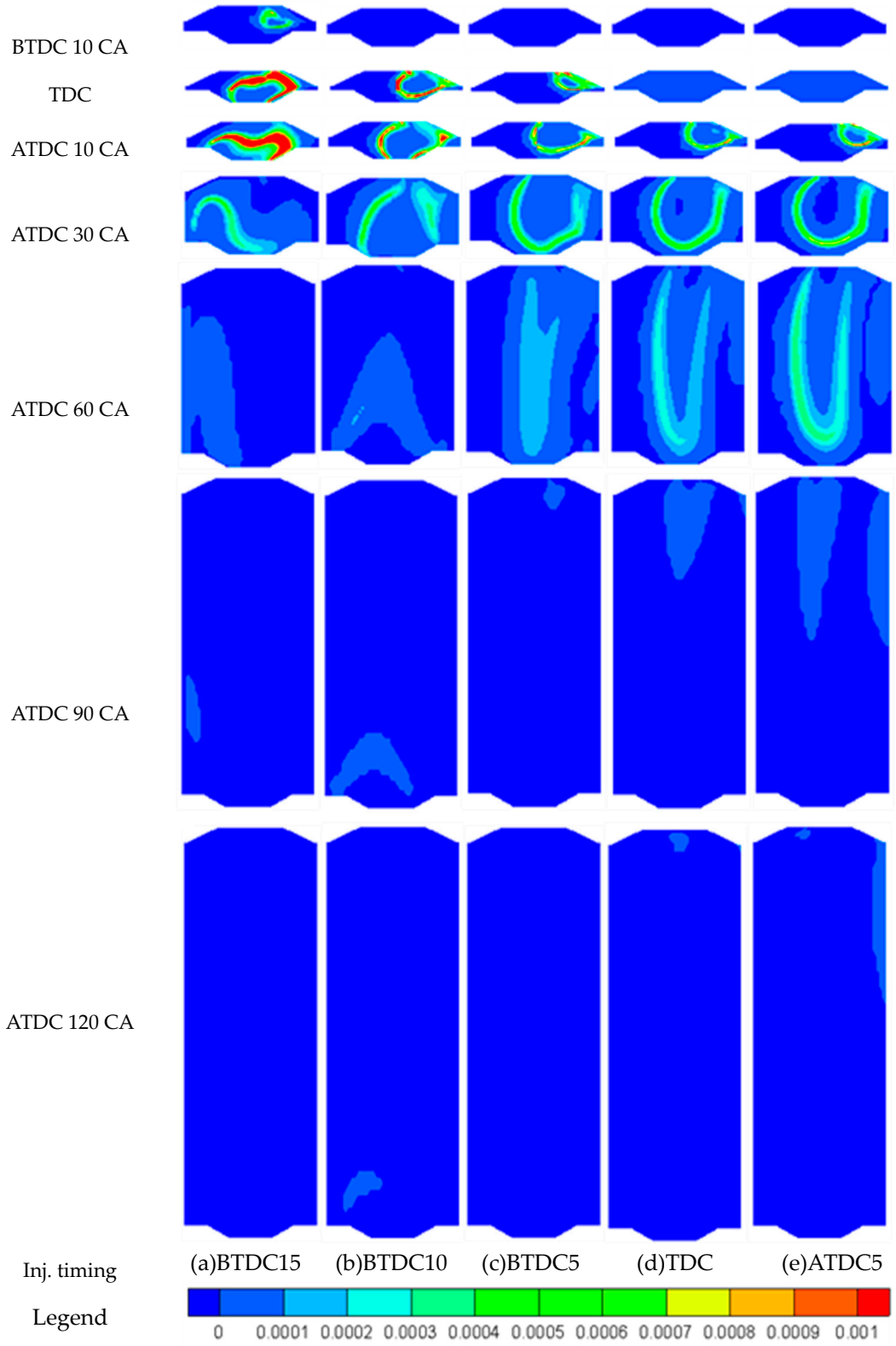

Figure 21. OH radical distribution at the center section of combustion chamber.

In Figures 22 and 23, the OH volume fraction across the crank angle and the OH fraction at the exhaust point are presented. These figures highlight that the highest value of OH concentration exhibits a difference of more than 5 times depending on the injection timing. This significant variation underscores the substantial impact of injection timing on the combustion rate during the main combustion period.

Preprints (www.preprints.org) | NOT PEER-REVIEWED | Posted: 22 November 2023 doi:10.20944/preprints202311.1373.v1

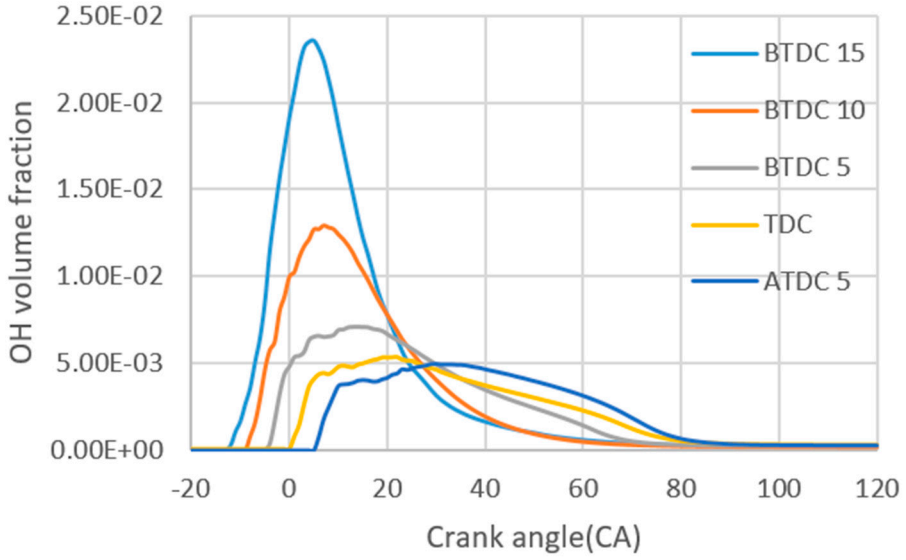

Figure 22. OH radical volume fraction with injection timing variation.

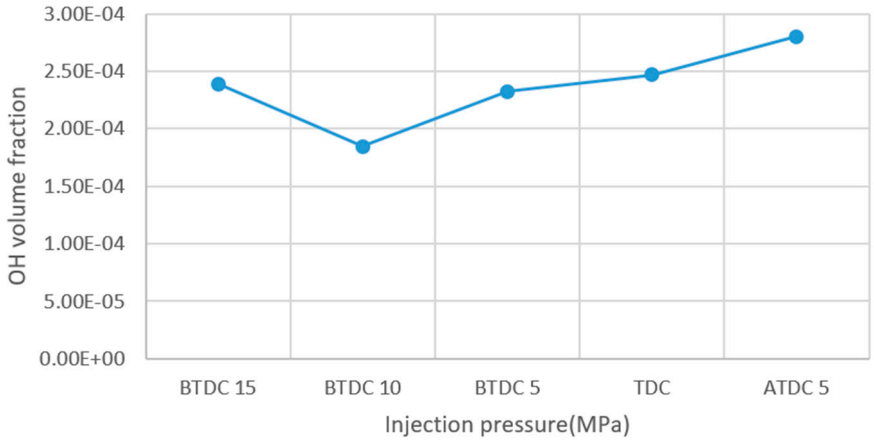

Figure 23. OH radical volume fraction at the exhaust valve open with injection timing variation.

In Figures 24–26, the distribution of the CO (carbon monoxide) volume fraction, the total CO fraction across the crank angle, and the fraction at the time the exhaust valve opens is illustrated. When the injection timing is set before Before Top Dead Center (BTDC) 10, there is a concentration of high CO near the piston crown during the main combustion period. Conversely, when the injection timing is after BTDC 5, a low concentration of CO is widely distributed inside the combustion chamber.

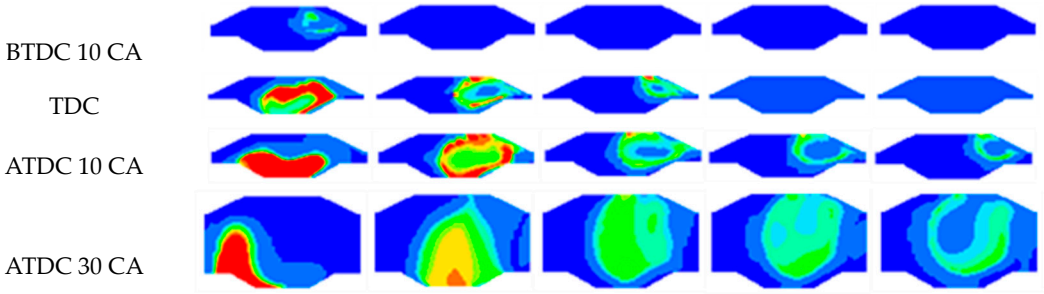

Preprints (www.preprints.org) | NOT PEER-REVIEWED | Posted: 22 November 2023 doi:10.20944/preprints202311.1373.v1

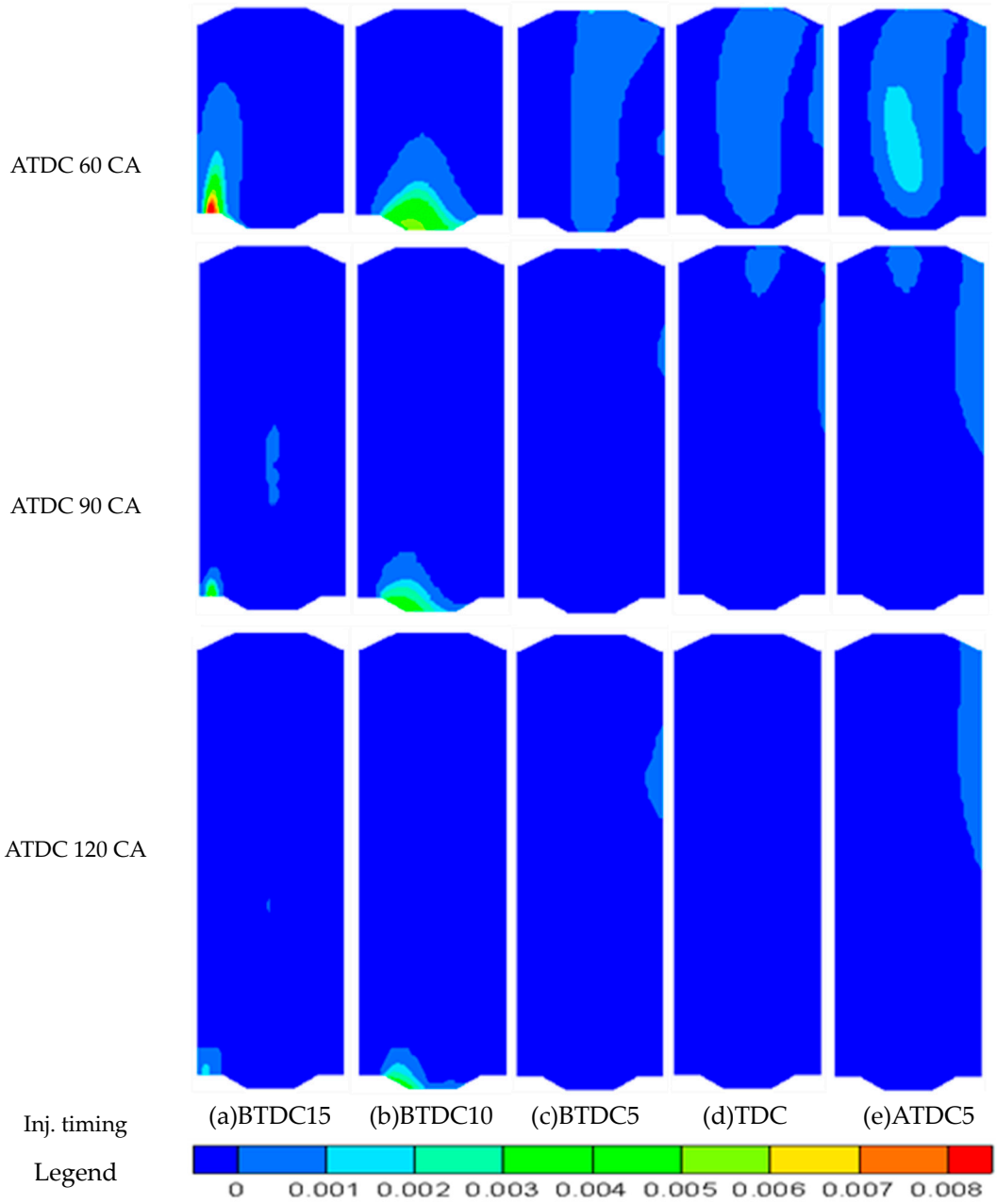

Figure 24. CO distribution at the center section of combustion chamber.

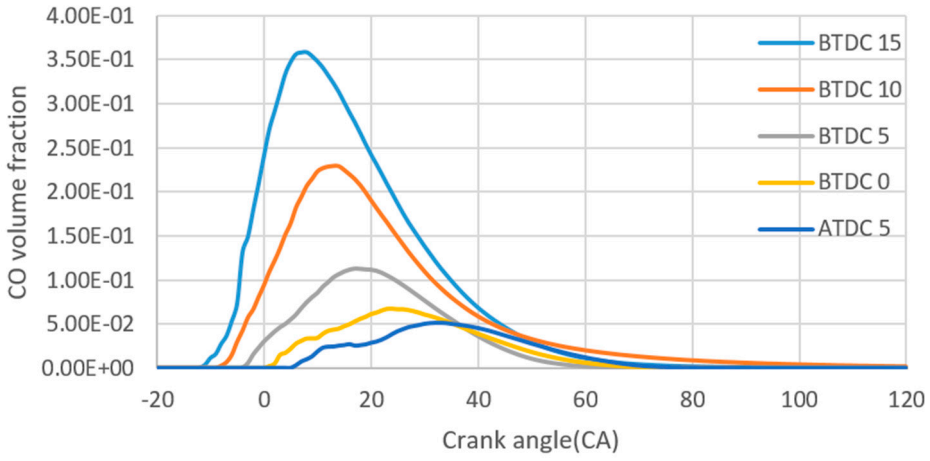

Figure 25. CO volume fraction with injection timing variation.

Preprints (www.preprints.org) | NOT PEER-REVIEWED | Posted: 22 November 2023 doi:10.20944/preprints202311.1373.v1

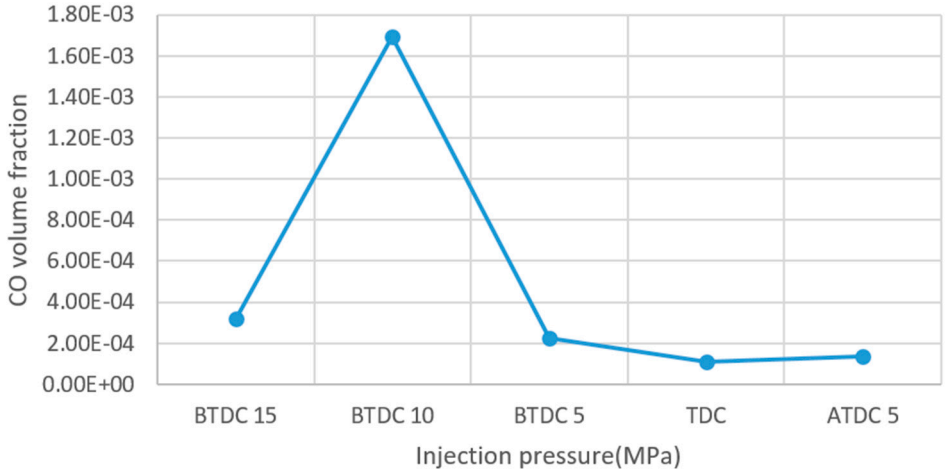

Figure 26. CO volume fraction at the exhaust valve open with injection timing variation.

In Figures 27–29, the distribution of nitrogen oxide, the average value in the cylinder, and the volume fraction of nitrogen monoxide at the time of exhaust are presented. The production of nitrogen oxides is influenced by the temperature of the combustion chamber, which is in turn determined by the fuel distribution and the burning rate of the flame front. The injection timing, directly related to the piston position, significantly impacts the combustion phenomenon. It determines the pressure, temperature, and fuel diffusion behavior of the combustion chamber during fuel injection. When the injection timing is advanced, a substantial amount of nitrogen oxide is generated, primarily due to the higher temperature experienced during the main combustion period.

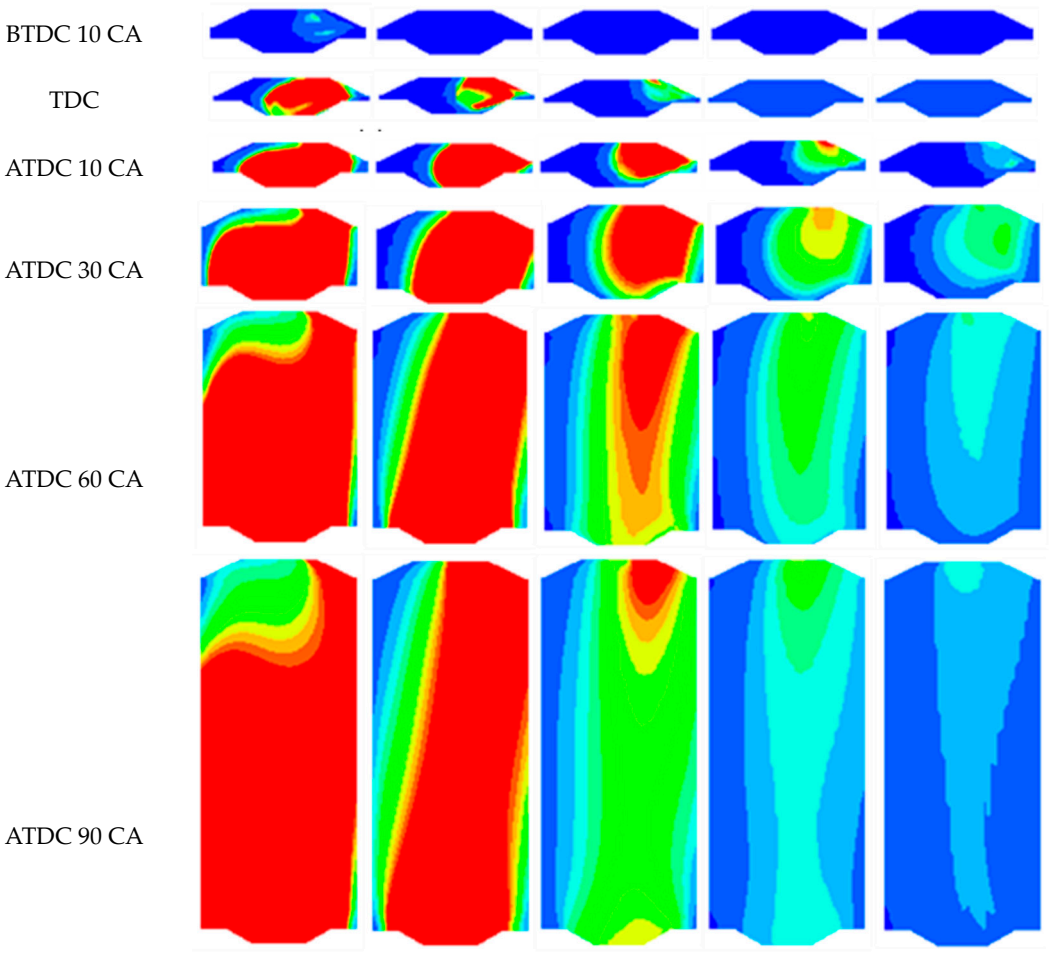

Preprints (www.preprints.org) | NOT PEER-REVIEWED | Posted: 22 November 2023 doi:10.20944/preprints202311.1373.v1

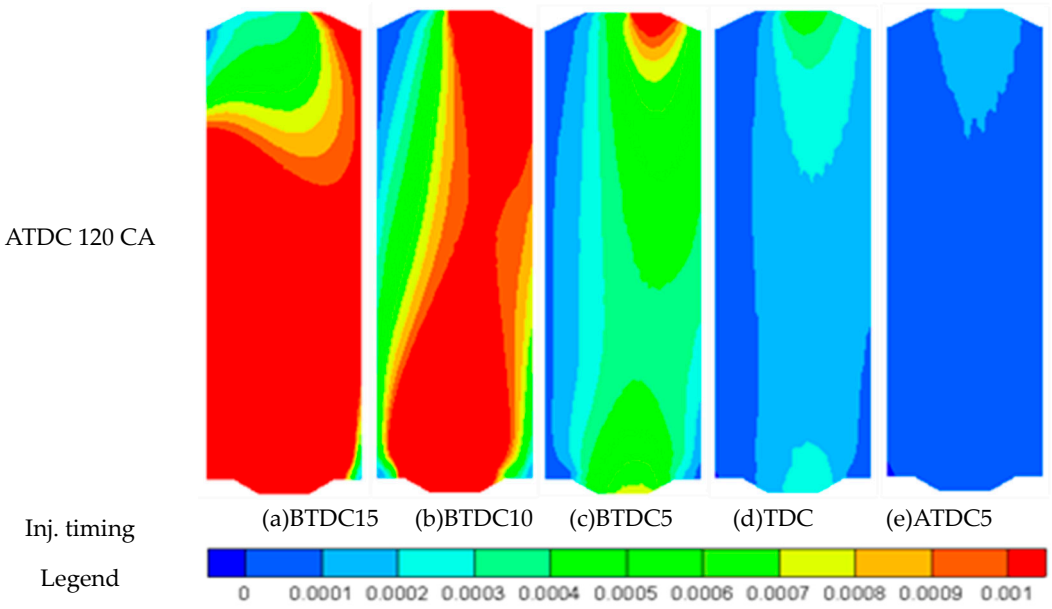

Figure 27. NO distribution at the center section of combustion chamber.

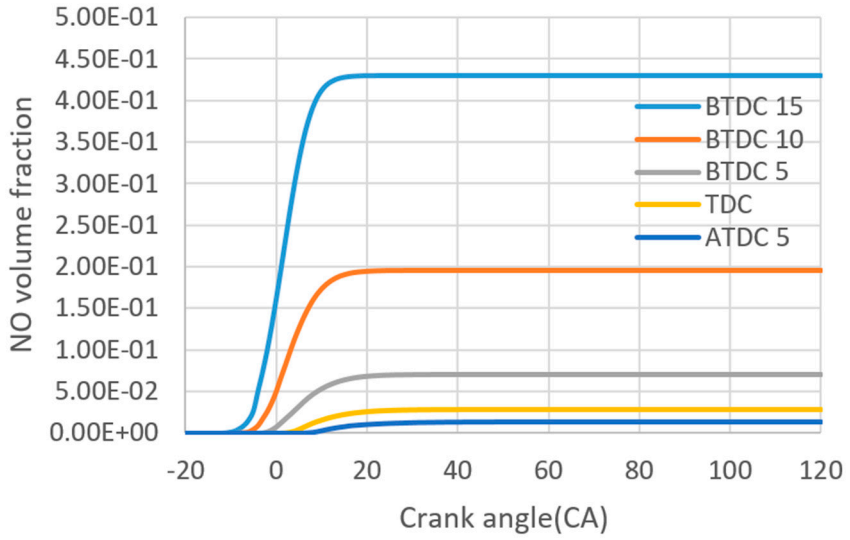

Figure 28. NO volume fraction with injection pressure variation.

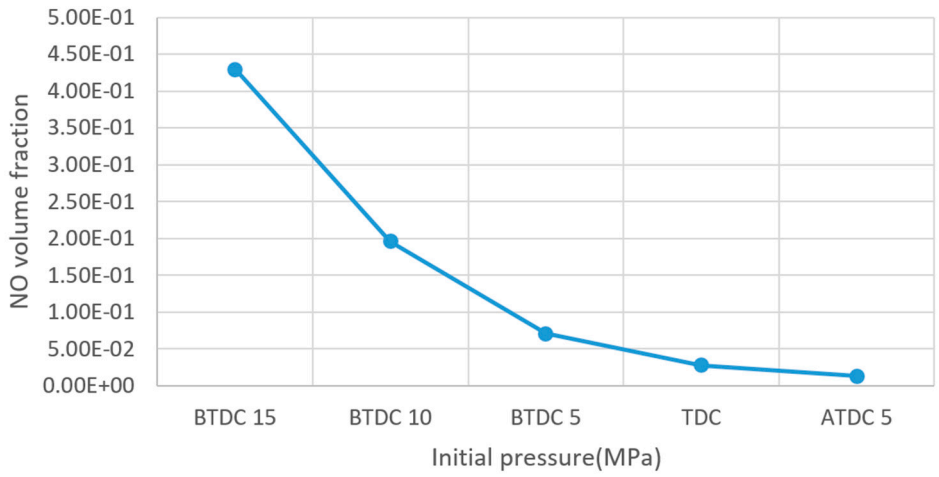

Preprints (www.preprints.org) | NOT PEER-REVIEWED | Posted: 22 November 2023 doi:10.20944/preprints202311.1373.v1

Figure 29. NO volume fraction at the exhaust valve open with injection pressure variation.

3.3. Injection Spray Angle

In Figures 30–32, the distribution of injected fuel, the average volume fraction in the cylinder, and the amount of remaining fuel at the time of exhaust are depicted. In the case of a small spray angle of 10 degrees, the spray's propagation is narrow and long. As the spray angle increases, the width of the spray widens, but the propagation distance decreases. With a small spray angle, the injected fuel propagates quickly to the piston crown, but this propagation is delayed with an increase in the spray angle. At the time of exhaust, the amount of residual fuel decreases as the injection angle increases, but there is an increase again at 50 degrees.

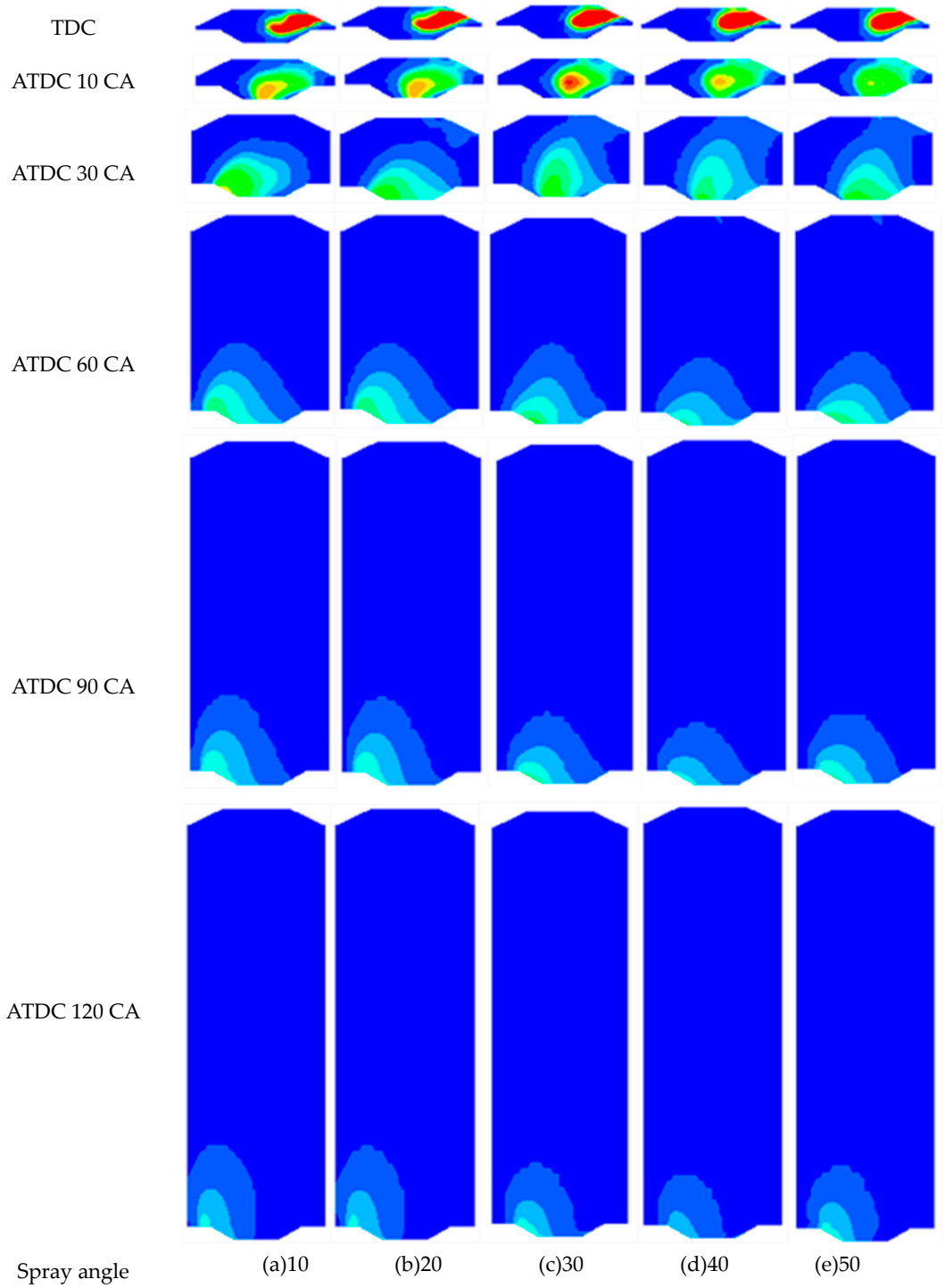

Preprints (www.preprints.org) | NOT PEER-REVIEWED | Posted: 22 November 2023 doi:10.20944/preprints202311.1373.v1

Figure 30. Fuel volume fraction distribution at the center section of combustion chamber.

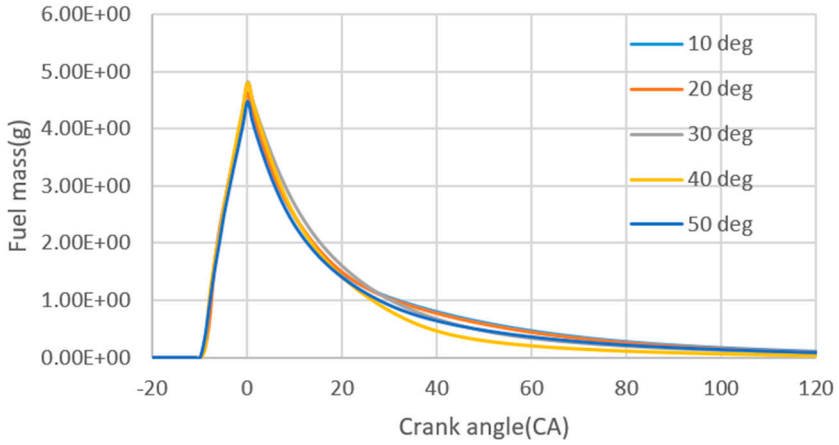

Figure 31. Residual fuel mass with injection spray angle variation.

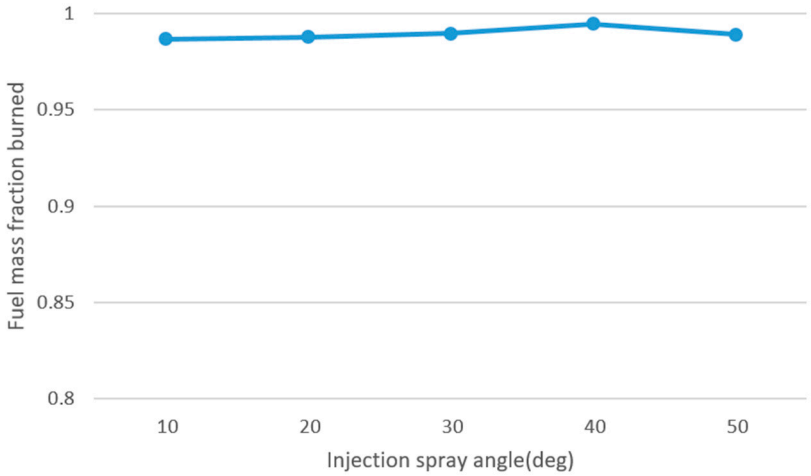

Figure 32. Fuel mass fraction burned at the exhaust valve open with injection spray angle variation.

In Figure 33, the temperature distribution in the combustion chamber is depicted, and Figure 34 illustrates the cylinder pressure. The hot region, caused by the heat of the flame front, expands more widely with an increase in the spray angle. When the spray angle is small, a thick distribution of high temperature occurs near the flame surface during the initial combustion period. For spray angles of 30 degrees or more, the high-temperature area is reduced. However, when the spray angle is further increased to 50 degrees, the high-temperature area increases again. This effect is attributed to the fuel being concentrated narrowly and longitudinally with a small spray angle, while it is distributed widely as the spray angle increases. If the spray angle is excessively increased, the propagation of the fuel is reduced, and the injected fuel is not spread widely, leading to concentrated combustion. Notably, the change in cylinder pressure does not exhibit a significant difference across these variations.

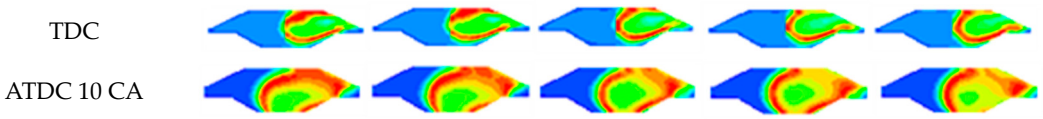

Preprints (www.preprints.org) | NOT PEER-REVIEWED | Posted: 22 November 2023 doi:10.20944/preprints202311.1373.v1

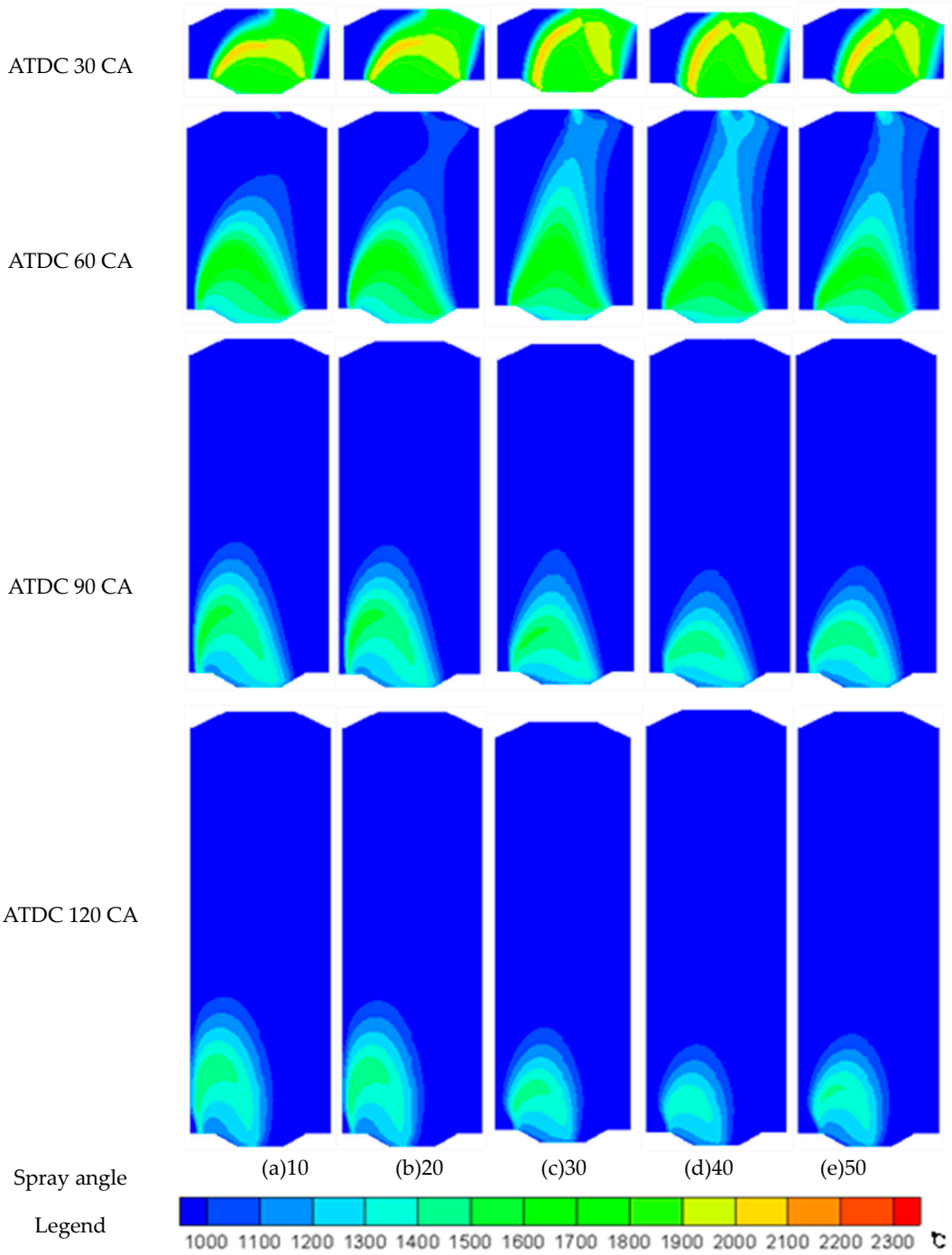

Figure 33. Temperature distribution at the center section of combustion chamber.

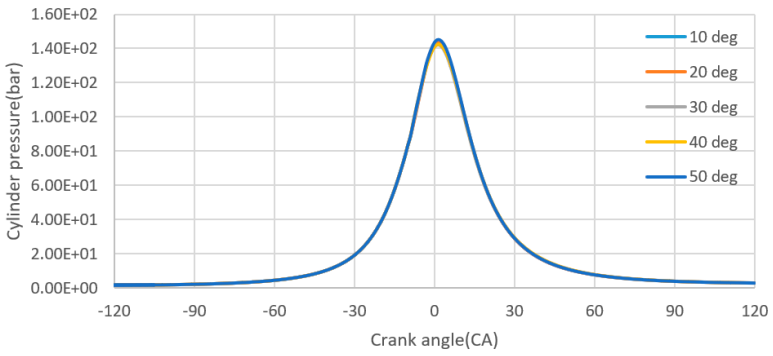

Preprints (www.preprints.org) | NOT PEER-REVIEWED | Posted: 22 November 2023 doi:10.20944/preprints202311.1373.v1

Figure 34. Cylinder pressure variation with fuel injection pressures.

In Figure 35, the distribution of OH radicals, which are intermediate products of combustion at the flame front, is presented. Figures 36 and 37 illustrate the change in the total OH volume fraction across the crank angle and its value at the exhaust timing, respectively. OH radicals, which were long and narrowly distributed when the spray angle was small, gradually decrease in propagation distance and spread widely as the spray angle increases. The maximum value of OH radicals, appearing around After Top Dead Center (ATDC) 10, shows the lowest value at a spray angle of 30 degrees and the highest value at a spray angle of 10 degrees. This indicates that the distribution and concentration of OH radicals are influenced by the spray angle, with different propagation characteristics.

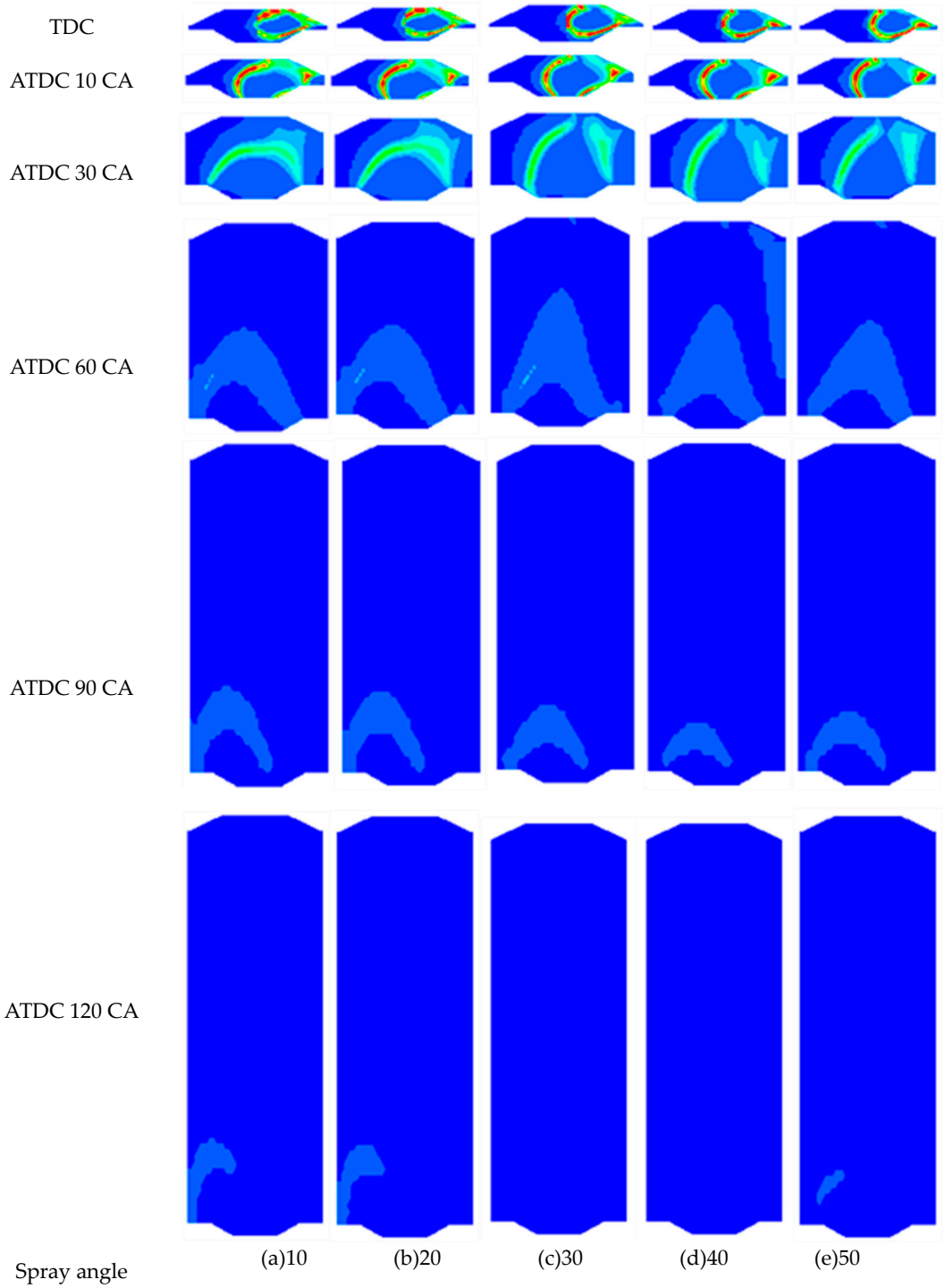

Preprints (www.preprints.org) | NOT PEER-REVIEWED | Posted: 22 November 2023 doi:10.20944/preprints202311.1373.v1

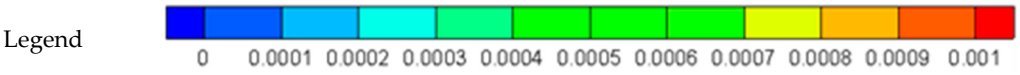

Figure 35. OH radical distribution at the center section of combustion chamber.

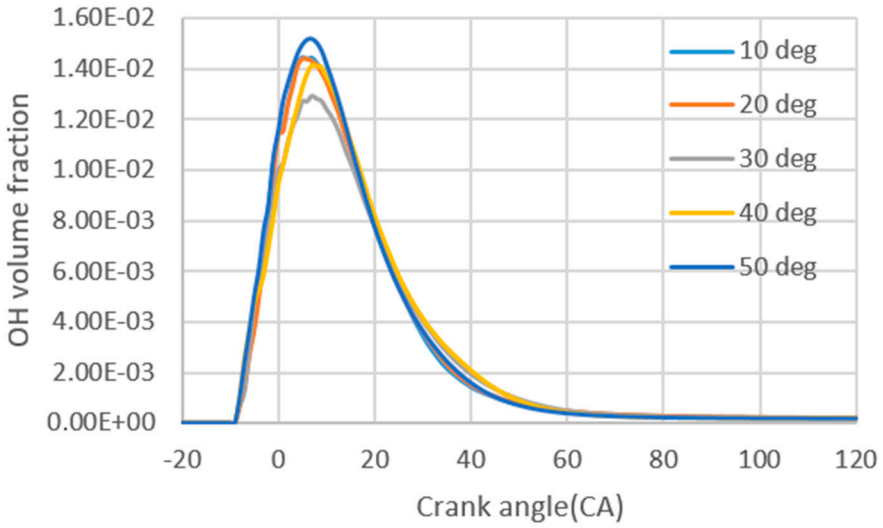

Figure 36. OH radical volume fraction with injection spray angle variation.

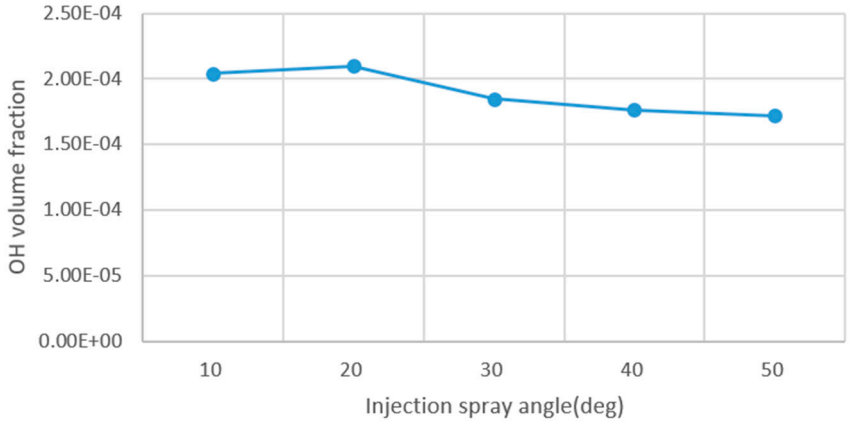

Figure 37. OH radical volume fraction at the exhaust valve open with injection spray angle variation.

In Figures 38–40, the distribution of the CO (carbon monoxide) volume fraction across the crank angle, the total CO fraction across the crank angle, and the fraction at the exhaust timing are displayed. Similar to the distribution of OH, the distribution of CO also exhibits high concentration when the spray angle is small and low concentration between 30 and 40 degrees. The maximum value of the CO volume fraction shows the lowest value between 30 and 40 degrees. The amount of CO remaining at the exhaust time exhibits the lowest value at the spray angle of 40 degrees. This suggests that the spray angle influences the distribution and concentration of CO, with varying levels at different spray angles.

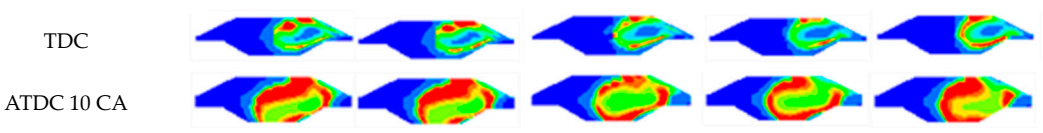

Preprints (www.preprints.org) | NOT PEER-REVIEWED | Posted: 22 November 2023 doi:10.20944/preprints202311.1373.v1

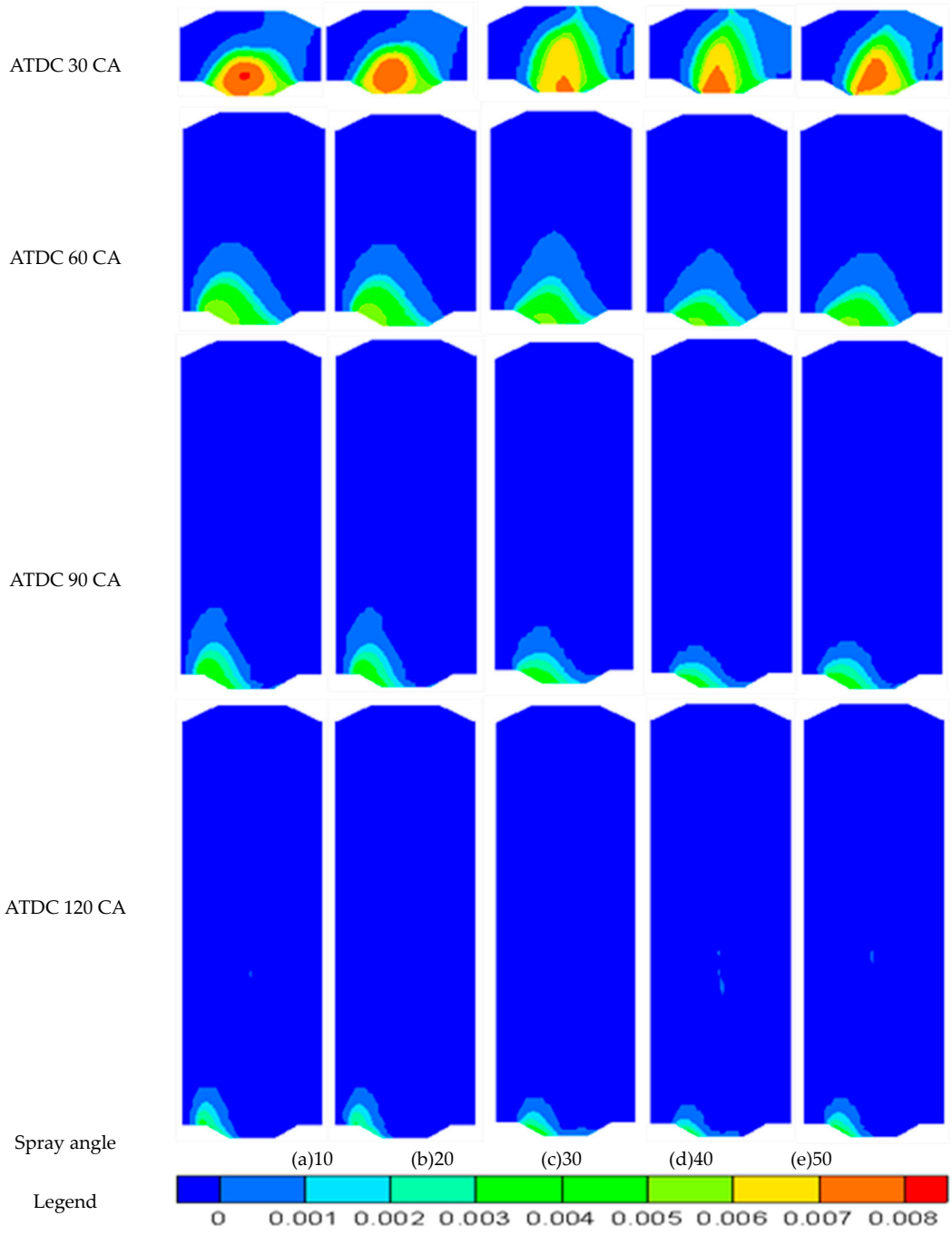

Figure 38. CO distribution at the center section of combustion chamber.

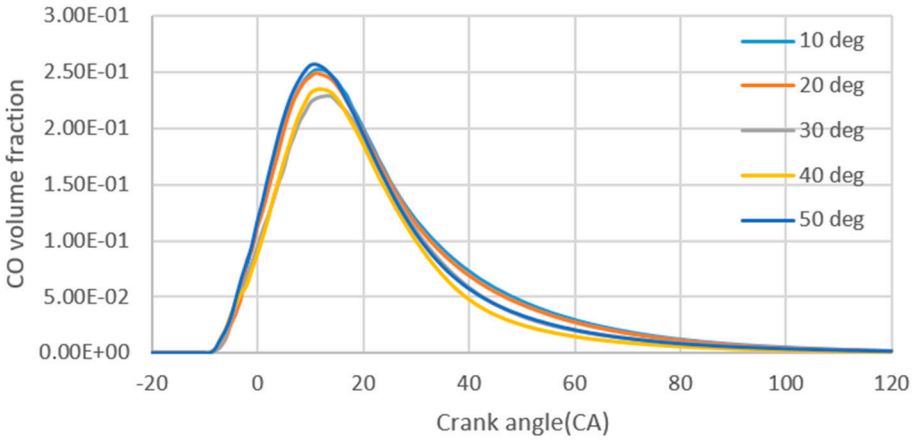

Preprints (www.preprints.org) | NOT PEER-REVIEWED | Posted: 22 November 2023 doi:10.20944/preprints202311.1373.v1

Figure 39. CO volume fraction with injection spray angle variation.

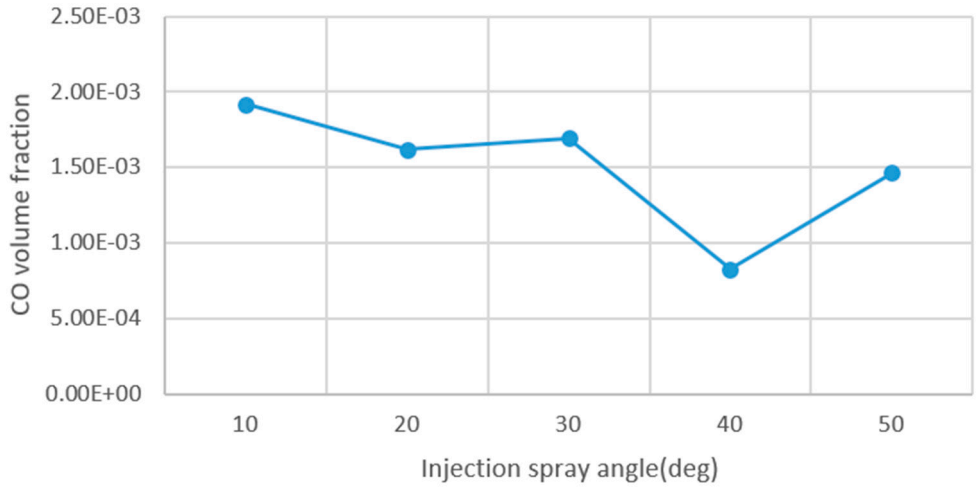

Figure 40. CO volume fraction at the exhaust valve open with injection spray angle variation.

In Figures 41–43, the distribution of nitrogen oxides across the crank angle, the fraction of the total nitrogen oxides across the crank angle, and the residual values at the time of opening the exhaust valve are presented. Nitrogen oxides are rapidly generated near Top Dead Center (TDC). The value of nitrogen oxides increases significantly when the spray angle is small or very large. The lowest value of nitrogen oxides is observed between the spray angle of 30 and 40 degrees. The observed trends suggest that if the spray angle is too small or too large, the injected fuel is not spread widely, leading to an intensive burning and a rise in temperature, which contributes to the increased generation of nitrogen oxides.

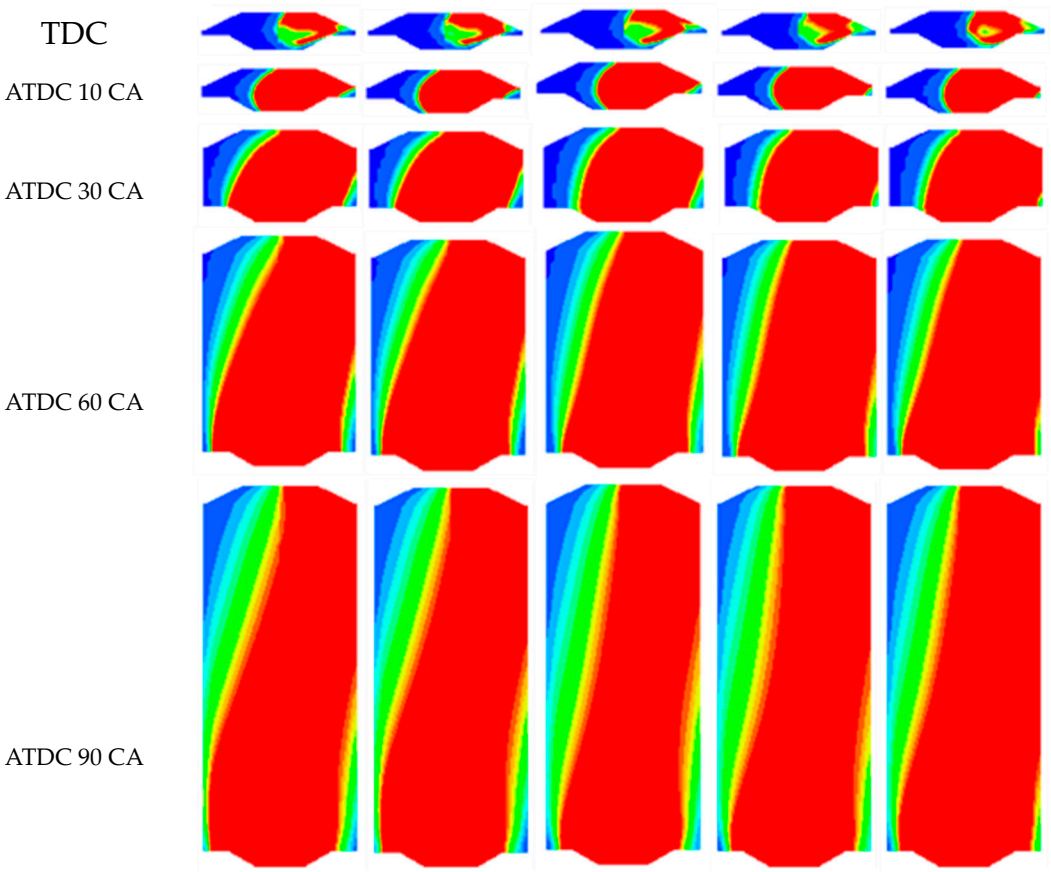

Preprints (www.preprints.org) | NOT PEER-REVIEWED | Posted: 22 November 2023 doi:10.20944/preprints202311.1373.v1

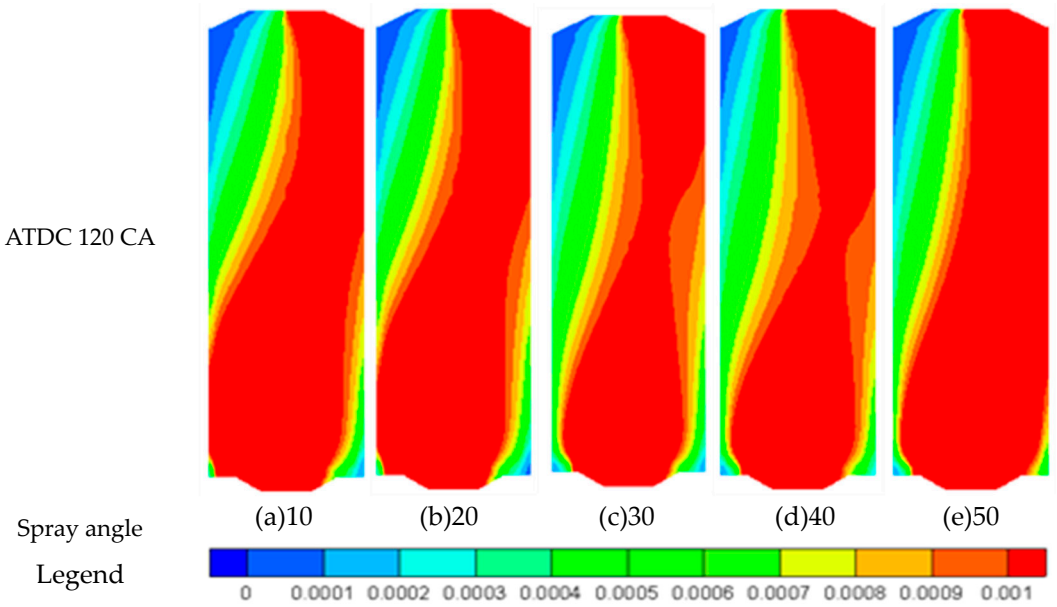

Figure 41. NO distribution at the center section of combustion chamber.

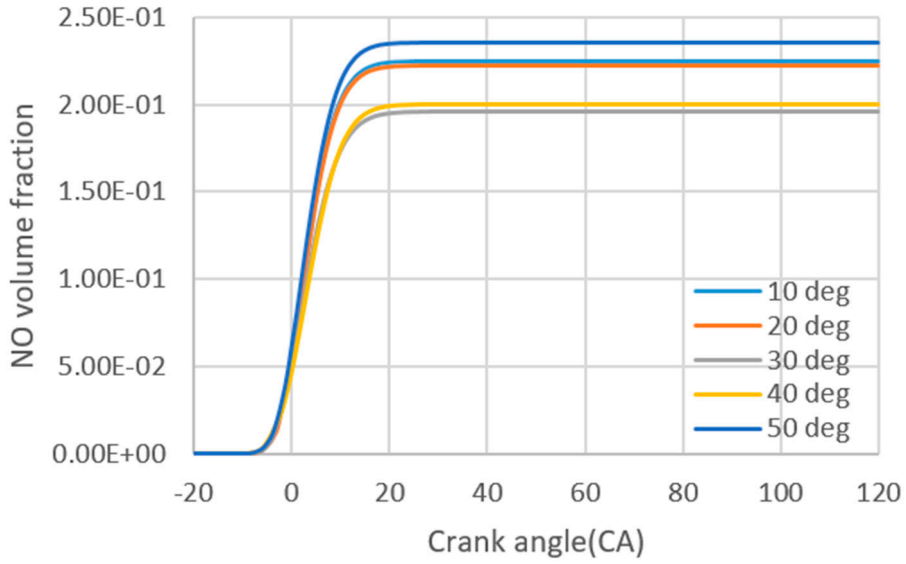

Figure 42. NO volume fraction with injection spray angle variation.

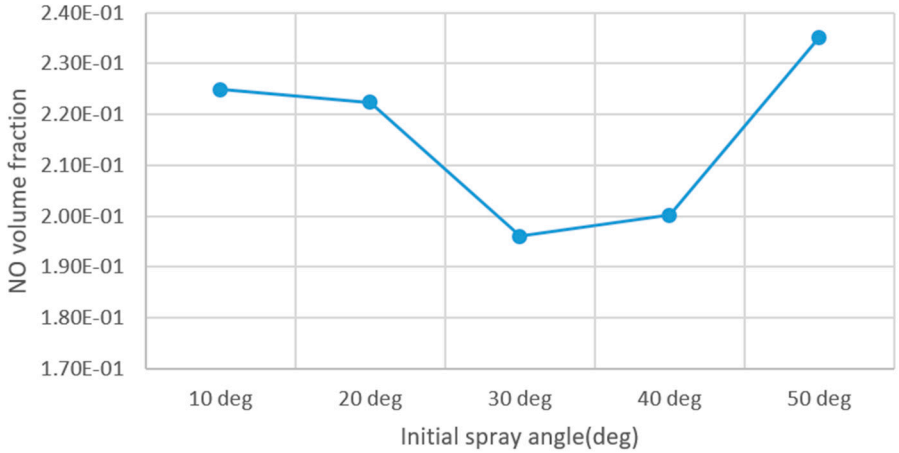

Preprints (www.preprints.org) | NOT PEER-REVIEWED | Posted: 22 November 2023 doi:10.20944/preprints202311.1373.v1

Figure 43. NO volume fraction at the exhaust valve open with injection spray angle variation.

4. Discussion

4.1. Fuel Spray Behavior

In Figure 44, the fuel distribution during a period of significant spray behavior change is depicted to analyze the effect of variation in injection conditions. When the injection pressure is less than 40 MPa, a high-concentration fuel area exists near the piston upper surface up to After Top Dead Center (ATDC) 10. However, when the injection pressure is 80 MPa or more, this high-concentration area is significantly reduced. The high-concentration region during the most active combustion phase contributes to a decrease in combustion efficiency and an increase in unburned emissions. The effect of injection timing on fuel distribution is observed to be much greater than the effect of injection pressure. Changes in cylinder pressure and space, influenced by the piston's movement, significantly impact fuel distribution characteristics based on injection timing. When the injection starts before Before Top Dead Center (BTDC) 10, the injected fuel is distributed in the high-temperature and high-pressure space while the piston rises, resulting in quick combustion. Consequently, only a small amount of residual fuel is left on the upper left side of the piston at ATDC 30. When the injection timing is delayed, the injected fuel is widely distributed in the widened space as the piston descends. However, combustion slows down as the temperature and pressure decrease with the descent of the piston, leading to a significant amount of unburned fuel remaining in the combustion chamber up to ATDC 60. The spray angle influences the spray distance and width of the fuel. A smaller spray angle results in increased spray distance and decreased width, while a larger spray angle leads to decreased spray distance and increased width. However, the effect of spray angle on fuel behavior is deemed insignificant compared to the impact of injection pressure and injection timing.

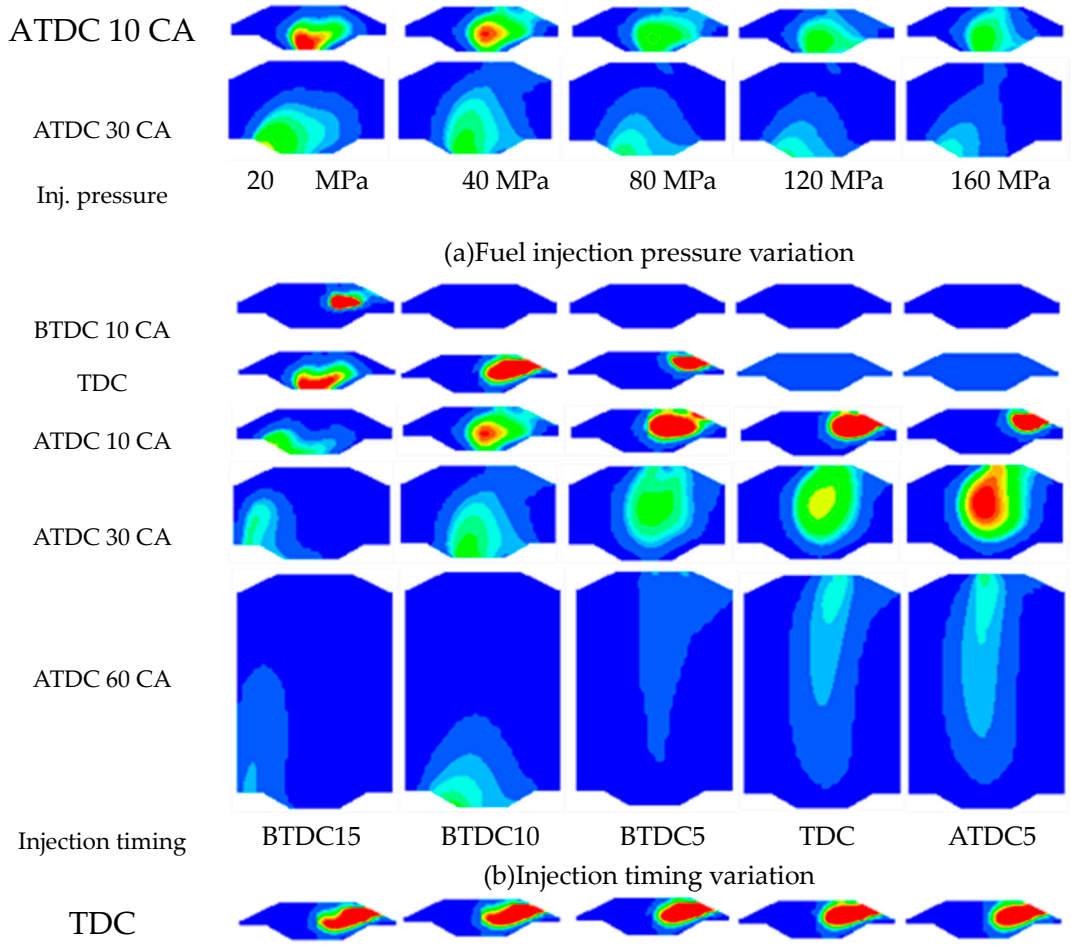

Preprints (www.preprints.org) | NOT PEER-REVIEWED | Posted: 22 November 2023 doi:10.20944/preprints202311.1373.v1

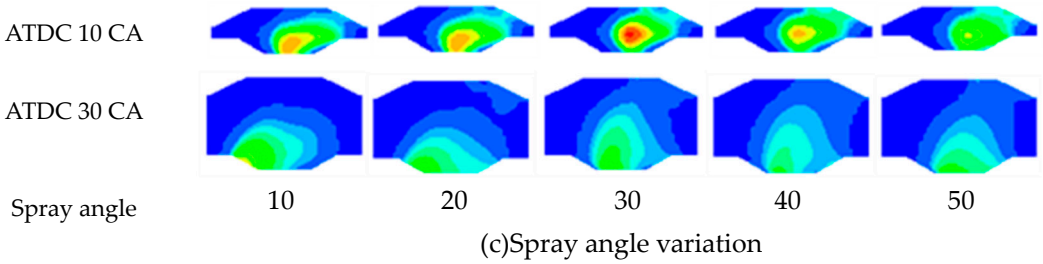

Figure 44. Fuel volume fraction distributions with fuel injection condition variation.

In Figure 45, the mass fraction of burned fuel to injected fuel is illustrated based on injection pressure, injection timing, and spray angle at the time the exhaust valve is opened. Under the operating conditions of the target engine (injection pressure of 40 MPa, injection timing of Before Top Dead Center (BTDC) 10, and injection angle of 30 degrees), 99% of the total injected fuel was burned. Excluding the case where the injection pressure is 20 MPa and the case where the spray angle is below 20 degrees, all other cases exhibit a combustion rate exceeding 99%. The fuel injection amount applied in this study is 70% of the injection amount at maximum power (MCR), ensuring sufficient oxygen is available to burn all the fuel. The area where the fuel is distributed and the concentration of the fuel are identified as crucial factors determining the combustion rate. When the fuel injection pressure is low and the spray angle is small, the injected fuel does not spread widely, creating a high-concentration area. Consequently, the amount of unburned fuel increases until the exhaust time under such conditions.

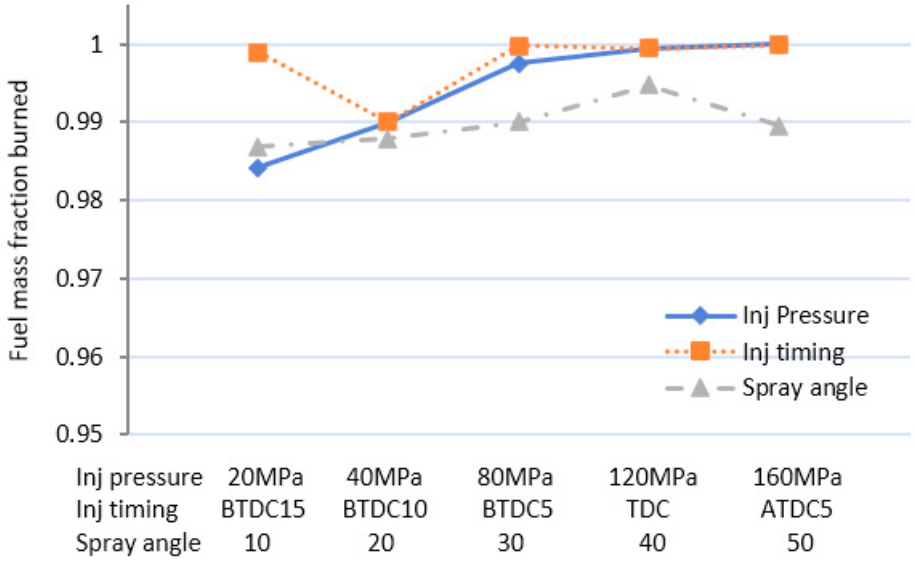

Figure 45. Fuel mass fraction burned at the exhaust valve open with Injection pressure, injection timing and spray angle variation.

4.2. Flame Propagation Behavior

In Figure 46, the distribution of OH radicals is depicted, considering variations in fuel injection pressure, injection timing, and spray angle. OH radicals are intermediate products of combustion generated at the flame surface, reflecting the flame propagation behavior. Fuel injection pressure significantly influences the distribution of fuel and its mixing with the surrounding air, consequently affecting flame behavior. As injection pressure increases, the flame area expands, leading to higher concentrations of OH radicals. This results in an increased combustion rate and heat release rate, contributing to elevated temperatures around the flame front. The impact of injection timing varies depending on whether fuel is injected during the compression or expansion process. For instance, when fuel is injected at Before Top Dead Center (BTDC) 15, completing injection before the piston

 doi:10.20944/preprints202311.1373.v1

reaches Top Dead Center (TDC), the main combustion occurs during the compression process, resulting in a high concentration of OH radicals forming a thick flame front. Delaying injection timing leads to lower OH concentration due to decreased cylinder pressure and temperature as the piston descends. However, OH radicals are more widely distributed in the expanded space. The spray angle's influence on OH distribution is not as significant as the effects of injection pressure and timing. Increasing the spray angle causes the OH distribution to expand, enlarging the flame front. Selecting appropriate conditions, considering factors like thermal efficiency and exhaust emissions, is crucial when designing combustion systems, as the fuel injection timing, closely tied to piston movement, has a substantial impact on flame propagation.

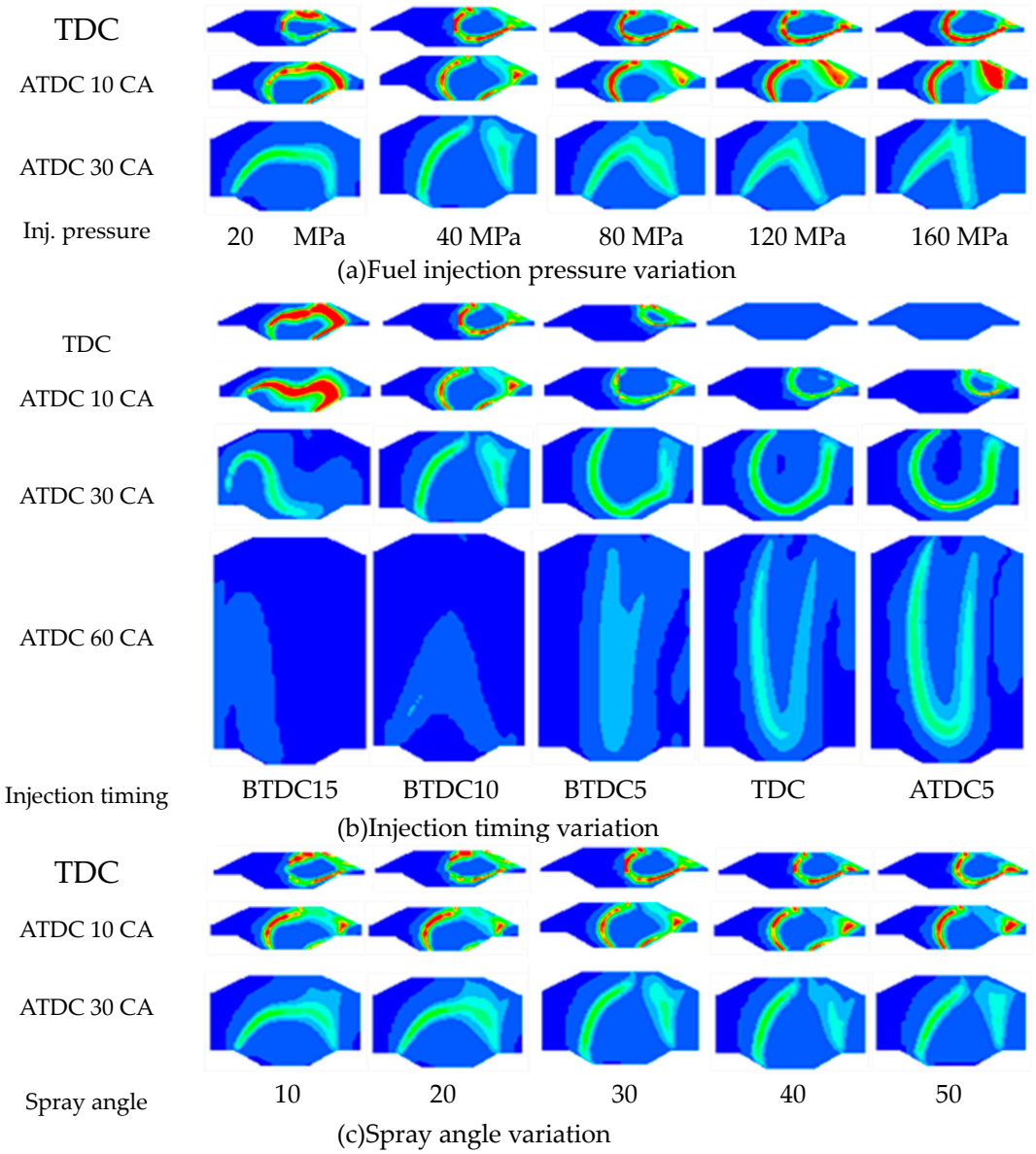

Figure 46. OH radical volume fraction distributions with fuel injection condition variation.

In Figure 47, the maximum value of the OH volume fraction is presented, illustrating the behavior of the flame front during peak combustion activity. Elevating the fuel injection pressure or advancing the injection timing results in a significant acceleration of the flame propagation speed. This leads to a higher maximum value of the OH volume fraction, indicating a more intense combustion process. Conversely, delaying the fuel injection timing significantly reduces the flame propagation speed. This is manifested in a lower maximum value of the OH volume fraction,

Preprints (www.preprints.org) | NOT PEER-REVIEWED | Posted: 22 November 2023 doi:10.20944/preprints202311.1373.v1

indicating a less vigorous combustion process. Changes in the spray angle have a relatively small impact on combustion compared to variations in injection pressure and timing.

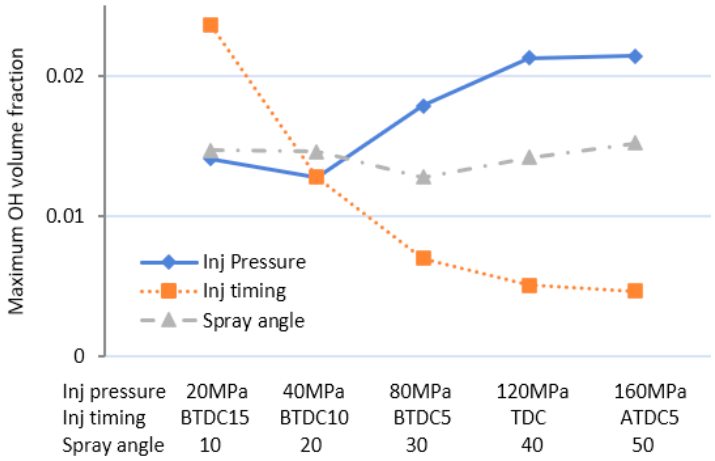

Figure 47. Maximum OH radical volume fraction with fuel injection condition variation.

Figure 48 shows how carbon monoxide distribution changes with variations in fuel injection pressure, fuel injection timing, and spray angle. Carbon monoxide levels rise at the onset of combustion and diminish as complete burning occurs. Under high-temperature conditions with adequate air and time, carbon monoxide is entirely consumed. With low fuel injection pressure, carbon monoxide distribution is minimal at ATDC 10 during main combustion. Even at ATDC 60, as combustion concludes, a substantial amount of CO persists. Conversely, higher injection pressure leads to a concentrated carbon monoxide presence around ATDC 10 during active combustion, with a rapid decline thereafter.

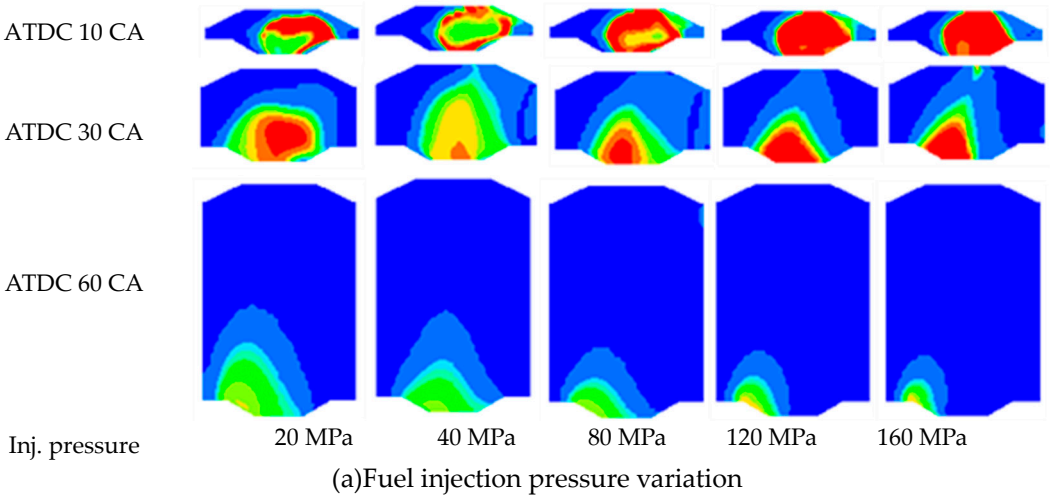

(a)Fuel injection pressure variation

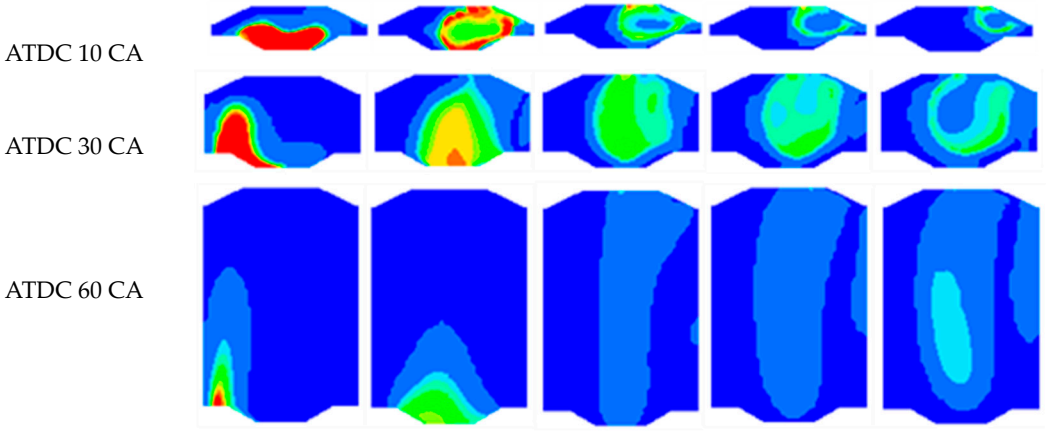

Preprints (www.preprints.org) | NOT PEER-REVIEWED | Posted: 22 November 2023 doi:10.20944/preprints202311.1373.v1

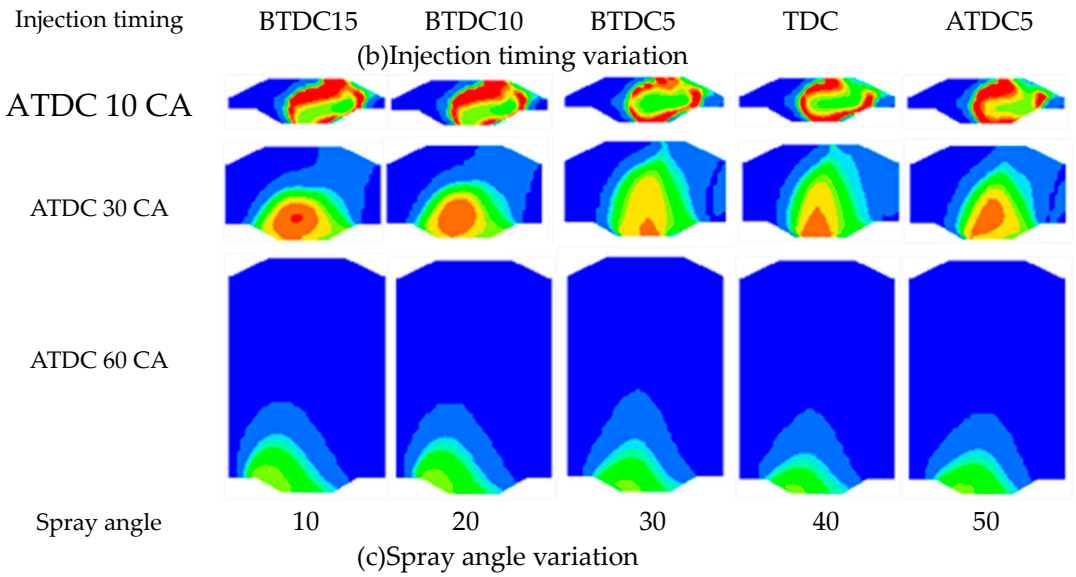

Figure 48. CO volume fraction distributions with fuel injection condition variation.

In the case of early injection timing before BTDC 10, the injection is completed while the piston is rising. This results in combustion near the upper surface of the piston, leading to the distribution of carbon monoxide in that area. Conversely, when injection starts after BTDC 5, fuel is injected until after top dead center, causing carbon monoxide to be widely distributed in the expanding space as the piston descends. The variation in fuel injection timing impacts combustion chamber temperature and space during compression and expansion, influencing the behavior of carbon monoxide generation and extinction. For instance, at BTDC 15, main combustion occurs during compression, leading to complete combustion and the disappearance of carbon monoxide, even though the fuel burns near the upper part of the piston and cylinder wall in a low-temperature state. After 5 degrees BTDC, where injection occurs during piston expansion, the injected fuel is distributed in the central space of the combustion chamber, separate from the low-temperature wall surface. This results in complete combustion and the disappearance of carbon monoxide. However, when injection starts at BTDC 10 and ends at TDC, the injected fuel is distributed over the low-temperature piston upper surface. As the piston moves down, a significant amount of carbon monoxide is present on the upper surface of the piston.

The spray angle influences the spread and distribution of fuel. With an increasing spray angle, the injected fuel is dispersed more widely, expanding the combustion area. Consequently, a larger spray angle tends to reduce emissions of the incomplete combustion product, carbon monoxide. However, if the spray angle becomes excessively large, the propagation distance of the fuel decreases, leading to an increase in carbon monoxide emissions once again.

Figure 49 shows the carbon monoxide distribution upon opening the exhaust valve, showcasing changes in fuel injection pressure, injection timing, and spray angle. The emission of incompletely burned carbon monoxide during the exhaust phase is significantly influenced by fuel injection conditions. Increasing fuel injection pressure results in a substantial reduction in carbon monoxide emissions. However, the impact of injection timing and spray angle varies based on the conditions in the combustion chamber during the main combustion period. The emission of carbon monoxide reaches a minimal level when the injection pressure exceeds 80 MPa, and the spray angle is set at 40 degrees.

Preprints (www.preprints.org) | NOT PEER-REVIEWED | Posted: 22 November 2023 doi:10.20944/preprints202311.1373.v1

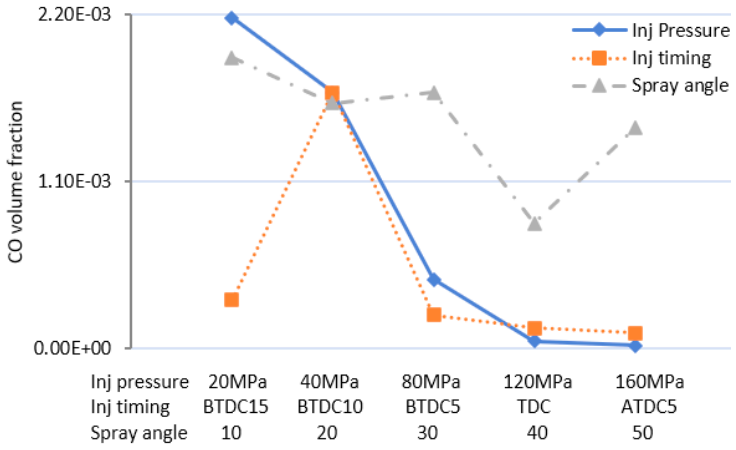

Figure 49. CO volume fraction at the exhaust valve open with Injection pressure, injection timing and spray angle variation.

Figure 50 shows the temperature distribution with variations in fuel injection pressure, timing, and spray angle, while Figure 51 shows the distribution of nitrogen oxide (NOx). The production of nitrogen oxides is directly influenced by flame temperature. NOx generated at high temperatures freezes rapidly after combustion, being discharged with the exhaust gas. The fuel injection pressure significantly influences fuel distribution and flame development. With increasing injection pressure, the combustion chamber's temperature rises markedly. Consequently, elevated injection pressure leads to higher temperatures and increased nitrogen oxide production, resulting in a substantial rise in NOx concentration. The timing of fuel injection, closely tied to piston movement, has a profound impact on combustion chamber pressure and temperature, significantly affecting NOx generation. Injection during the compression process, occurring in a high-temperature environment, yields high flame temperatures and a higher concentration of nitrogen oxides. Conversely, injection during the expansion stroke, in a lower-temperature atmosphere, reduces flame temperature and greatly decreases nitrogen oxides. The spray angle also plays a role; when too small or too large, it increases nitrogen oxides due to heightened local flame temperatures.

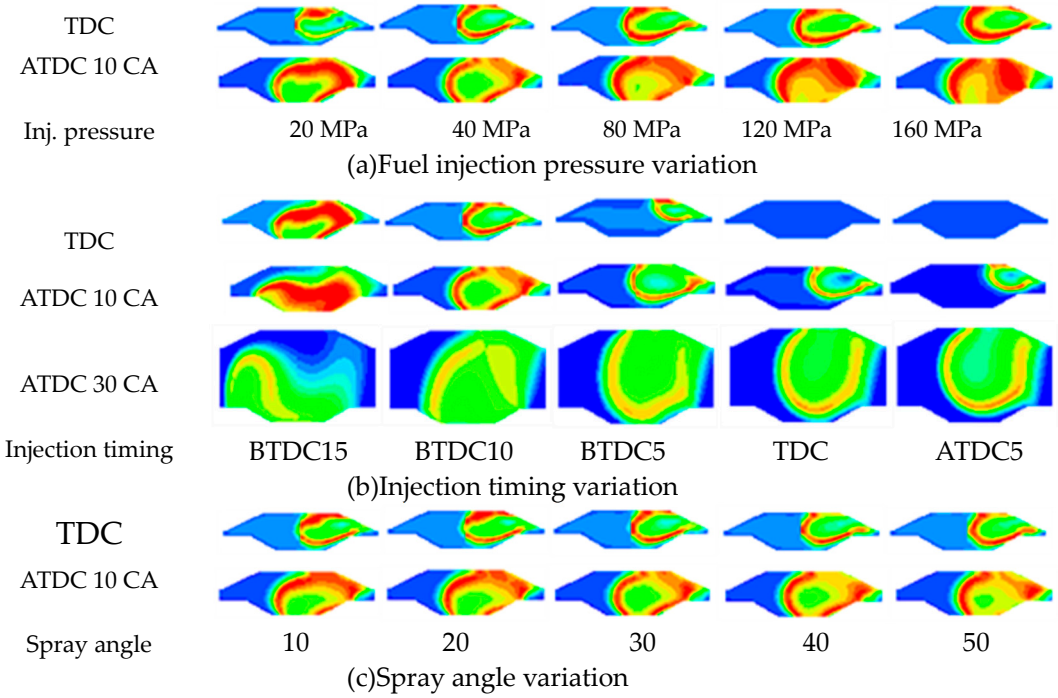

Figure 50. Temperature distributions with fuel injection condition variation.

Preprints (www.preprints.org) | NOT PEER-REVIEWED | Posted: 22 November 2023 doi:10.20944/preprints202311.1373.v1

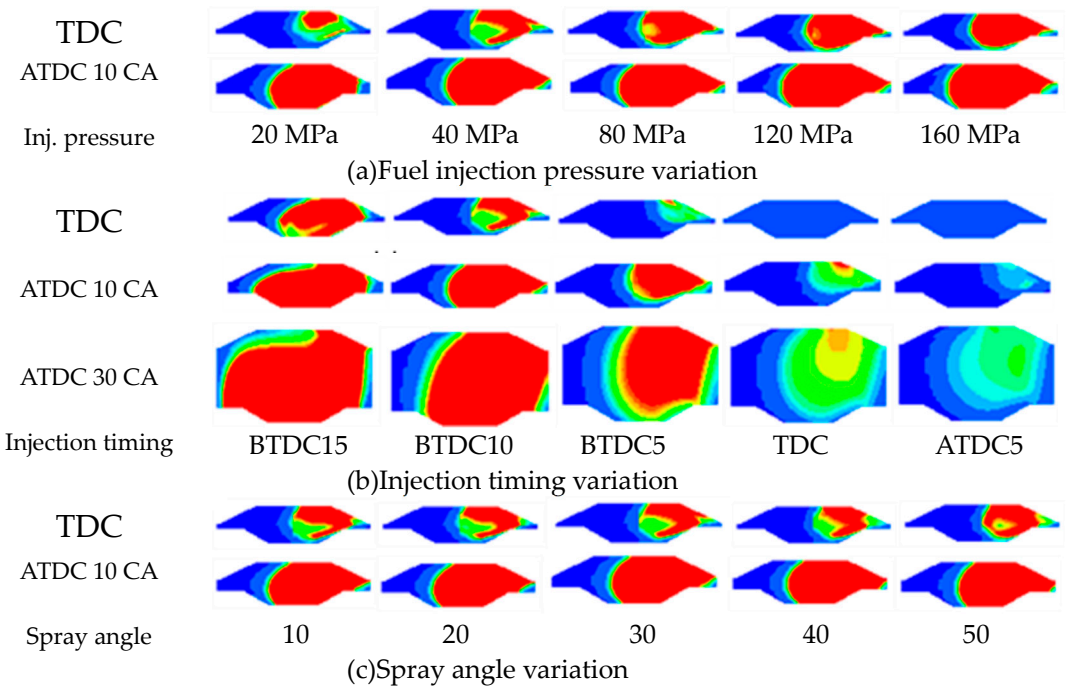

Figure 51. NO volume fraction distributions with fuel injection condition variation.

Figure 52 shows the volume fraction of nitrogen oxide when the exhaust valve opens, considering changes in fuel injection pressure, injection timing, and spray angle. The generation of nitrogen oxide is significantly influenced by injection timing and pressure, with relatively less impact from changes in the spray angle. Emissions of nitrogen oxides increase by over 70% when the injection pressure exceeds 120 MPa. An advanced injection timing, particularly at BTDC 15, results in a substantial 115% increase in nitrogen oxide emissions. Regarding the spray angle, the values remain low within the range of 30 to 40 degrees.

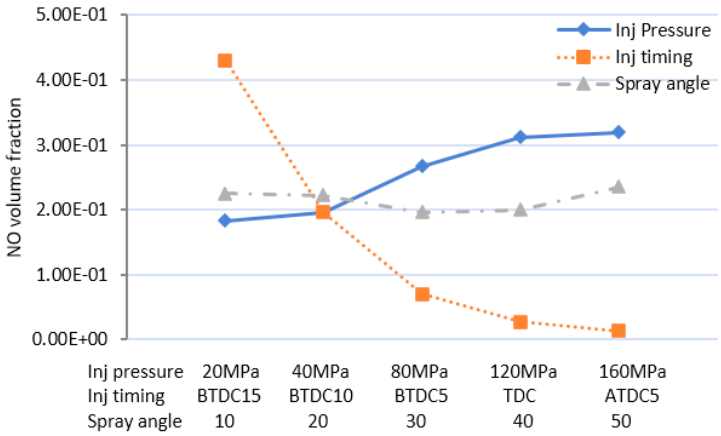

Figure 52. NO volume fraction at the exhaust valve open with Injection pressure, injection timing and spray angle variation.

5. Conclusions

This study analyzed the impact of fuel injection conditions on combustion behavior in marine diesel engines to enhance performance. The key findings are summarized as follows:

(1) Effect of fuel injection conditions on fuel behavior: At fuel injection pressures below 40 MPa, a concentrated fuel area forms near the upper piston surface, resulting in increased unburned fuel. However, beyond an injection pressure of 80 MPa, this high-concentration fuel area is notably diminished.

 doi:10.20944/preprints202311.1373.v1

The timing of fuel injection is intricately linked to the piston's movement. When injection commences before BTDC 10, it concludes while the piston is ascending. As a result, the injected fuel is dispersed in a high-temperature and high-pressure environment, undergoing rapid combustion. Conversely, with delayed injection timing, the injected fuel is widely distributed in the expanded space as the piston descends.

The variation in the spray angle impacts the distance and spread of the fuel spray. With a small spray angle, the injected fuel travels a greater distance and is distributed on the upper surface of the piston. As the spray angle increases, the spray's propagation distance decreases, forming a high-concentration area in the center of the combustion chamber.

A substantial amount of unburned fuel is produced when the injection pressure is below 40 MPa and the spray angle is below 20 degrees. However, this is significantly reduced when the injection pressure exceeds 80 MPa, and the spray angle is set to 40 degrees.

(2) Effect of fuel injection conditions on flame propagation: With an increase in fuel injection pressure, the flame area expands, and combustion speed accelerates. This results in a higher rate of heat release and an elevation in temperature around the flame face. Specifically, at injection pressures exceeding 80 MPa, the maximum value of the OH radical significantly increases, forming a local high-temperature region near the flame front.

The timing of fuel injection is directly linked to the piston's movement. When injection is completed before the piston reaches top dead center (TDC), primary combustion occurs under high-pressure and high-temperature conditions in the combustion chamber due to piston compression. Consequently, there is a very high concentration of OH radicals, resulting in the formation of a thick flame front. In contrast, with delayed fuel injection timing, the pressure and temperature decrease due to piston expansion. This leads to the widespread distribution of low-concentration OH along the piston's movement. As the spray angle increases, the distribution of OH expands, and the flame front widens considerably.

The flame propagation speed, as determined by the distribution of OH radicals, exhibits a very high value when the injection pressure exceeds 80 MPa and when the injection timing is set before BTDC 10.

(3) Effects of fuel injection conditions on carbon monoxide production: At low fuel injection pressure, there is a low concentration of carbon monoxide distributed during the main combustion period, and a substantial amount of CO persists even during the combustion-ending phase. In contrast, as the injection pressure increases, a high concentration of carbon monoxide is distributed during the main combustion period, followed by a rapid decrease in concentration.

When injection timing is advanced, and fuel is injected during the compression stroke, a significant amount of carbon monoxide is distributed on the upper surface of the piston. If the injection timing is set at BTDC 10, carbon monoxide remains on the upper surface of the piston until late in a low-temperature state. Conversely, when the injection timing is delayed, and injection begins after BTDC 5, fuel is injected until after top dead center (TDC). The injected fuel follows the expanding space as the piston descends, resulting in wide distribution of carbon monoxide. Despite the low temperature, the reaction continues with sufficient oxygen supply.

Increasing the spray angle widens the distribution of injected fuel, expanding the combustion area and reducing carbon monoxide. However, when the spray angle becomes excessively large, the propagation distance of the fuel is reduced, resulting in an increase in carbon monoxide. Carbon monoxide emissions show a very low value when the injection pressure exceeds 80 MPa and the spray angle is set at 40 degrees.

(4) Effect of fuel injection conditions on nitrogen oxide generation: With an increase in injection pressure, the temperature of the combustion chamber rises, leading to a significant increase in nitrogen oxide.

The timing of fuel injection, closely tied to the piston's movement, significantly influences the generation of nitrogen oxides as it impacts the pressure and temperature of the combustion chamber. Injection during the compression stroke leads to combustion in a high-temperature environment, resulting in the generation of high-concentration nitrogen oxides due to elevated flame temperatures.

Conversely, when injection occurs during the expansion stroke, combustion takes place in a low-temperature atmosphere, substantially reducing the generation of nitrogen oxides due to the lower flame temperature.

When the spray angle is too small or too large, a significant amount of nitrogen oxides is generated because the distribution of fuel becomes concentrated, leading to a rise in local flame temperature.

NOx emissions increased by over 70% with an injection pressure exceeding 120 MPa and rose to 115% with an advanced injection timing of BTDC 15. Nitrogen oxide emissions also increase when the spray angle is either too small or too large, but they decrease within the range of 30 to 40 degrees.

To enhance combustion efficiency and minimize incomplete combustion products, acceleration of combustion in a high-temperature environment is necessary. However, the challenge lies in the substantial generation of nitrogen oxides due to the elevated temperatures around the flame. Therefore, it is crucial to choose optimal conditions that take into account all combustion products. For the target engine in this study, the considered optimal injection conditions are an injection pressure of 80 MPa, an injection timing of BTDC 5, and a spray angle of 40 degrees.

Author Contributions: Conceptualization, K.P.; methodology K.P.; software, K.P.; validation, K.P. and K.P.; formal analysis, K.P.; investigation, K.P.; resources, K.P.; data curation, K.P.; writing-original draft preparation, K.P.; writing-review and editing, K.P.; supervision, K.P.; project administration, K.P.; The author has read and agreed to the published version of the manuscript.

Funding: Not applicable.

Institutional Review Board Statement: Not applicable.

Informed Consent Statement: Not applicable.

Data Availability Statement: Not applicable.

Conflicts of Interest: The authors declare no conflict of interest.

References

1. Gossling, S.; Meyer-Habighorst, C.; Humpe, A. A global review of marine air pollution policies, their scope and effectiveness. *Ocean and Costal Management* **2021**, 212.
2. FCCC/CP/2015/L.9/Rev.1. United Nations, United Nations Office at Geneva, Geneva. *UNFCCC*, **2015** Paris Agreement.
3. Masson-Delmotte, V.; Zhai, P.; Pörtner, H, O.; Roberts, D.; Skea, J; Shukla, P.R.; Pirani, A.; Moufouma-Okia, W.; Péan, C.; Pidcock, R.; Connors, S.; Matthews, J.B.R.; Chen, Y.; Zhou, X.; Gomis, M.I.; Lonnoy, E.; Maycock, T.; Tignor, M.; Waterfield, T. An IPCC Special Report on the impacts of global warming of 1.5°C above pre-industrial levels and related global greenhouse gas emission pathways, in the context of strengthening the global response to the threat of climate change, sustainable development, and efforts to eradicate poverty. *IPCC*, **2018**: Global Warming of 1.5°C.
4. International Maritime Organization. Fourth IMO GHG study **2020**. London, United Kingdom.
5. Marine Environment Protection Committee, 2020. Reduction of GHG Emissions from Ships. Fourth IMO GHG Study 2020 – Final Report.
6. IMO A.963 (23); IMO Policies and Practices Related to the Reduction of Greenhouse Gas Emission from ships, Dec. 2003.
7. IMO. Inclusion of Regulations on Energy Efficiency for Ships in MARPOL Annex V-Resolution MEPC.203(62); International Maritime Organization (IMO): London, UK, 2011
8. IMO, 2018. Resolution MEPC.304(72) (adopted on 13 April 2018), initial IMO strategy on reduction of GHG emissions from ships, IMO doc. MEPC 72/17/add.1, annex 11, 2018.
9. Kim, Hyungju; Koo, Kwi Yeon; Joung, Tae-Hwan, A study on the necessity of integrated evaluation of alternative marine fuels, *Journal of International Maritime Safety, Environmental Affairs, and Shipping*, **2020**, 4:2, 26-31.
10. Bouman, E. A.; Lindstad, E.; Rialland, A.I.; Strømman A.H. State-of-the-art Technologies, Measures, and Potential for Reducing GHG Emissions from Shipping–a Review. *Transportation Research Part D: Transport and Environment*, **2017**, 52: 408–421.
11. Azzara, A.; Rutherford, D.; Wang, H. Feasibility of IMO Annex VI Tier III implementation using Selective Catalytic Reduction. *Working Paper 2014-4, The International Council on Clean Transportation*, 2014.

12. Yang, Shaolong; Pan, Xinxiang; Han, Zhitao; Zhao, Dongsheng; Liu, Bojun; Zheng, Dekang; Yan, Zhijun. Removal of NOx and SO2 from simulated ship emissions using wet scrubbing based on seawater electrolysis technology. *Chemical Engineering Journal*, **2018**, 331, 8-15.
. Kuropyatnyk, S. Sagin. Exhaust Gas Recirculation as a Major Technique Designed to Reduce NOx Emissions from Marine Diesel Engines. Environmental Science, Engineering, 2019, DOI:10.17818/NM/2019/1.1
13. Li, T.; Susuki, M.; Ogawa, H. Effect of two-stage injection on unburned hydrocarbon and carbon monoxide emissions from ultra-high EGR low temperature diesel combustion. *Nippon Kikai Gakkai Ronbunshu*, **2010**, 766(76): 1004-1009.
14. Belousov, E. V.; Ageyev, M. S.; Sviridov, V. I. Exerting influence on operation of medium-speed marine diesel engine by injection of water into the working cylinder. *Dvigateli vnutrennego sgoraniya*, **2010**, 1: 40-43. (In Russian).
15. Zheng, M.; Asad, U.; Reader, G. T.; Tan, Y.; Wang, M. Energy efficiency improvement strategies for a diesel engine in low-temperature combustion. International Journal of Energy Research, **2009**, 33(1): 8-28. https://doi.org/10.1002/ er.1464
16. Sagin, S. V.; Semenov, O. V. Motor Oil Viscosity Stratification in Friction Units of Marine Diesel Motors. *American Journal of Applied Sciences*, **2016**, 13(2), 200-208.
17. Zablotsky, Yu. V.; Sagin, S. V. Maintaining Boundary and Hydrodynamic Lubrication Modes in Operating High-pressure Fuel Injection Pumps of Marine Diesel Engines. *Indian Journal of Science and Technology*, **2016**, 9(20), 208- 216.
18. Kumar, B. R.; Saravanan, S. Partially premixed low temperature combustion using dimethyl carbonate (DMC) in a DI diesel engine for favorable smoke/NOx emissions. *Fuel*, **2016**, 180(15): 396-406.
19. Miller Jothi, N. K.; Nagarajan, G.; Renganarayanan, S. LPG fueled diesel engine using diethyl ether with exhaust gas recirculation. *International Journal of Thermal Sciences*, **2008**, 47(4): 450-457.
20. Koci, P.; Plat, F.; Stepanek, J.; Kubicek, M.; Marek, M. Dynamics and selectivity of NOx reduction in NOx storage catalytic monolith. *Catalysis Today*, **2008**, 137(2-4): 253-260.
21. Aneggi, E.; de Leitenburg, C.; Trovarelli, A. Diesel soot combustion activity of ceria promoted with alkali metals. *Catalysis Today*, **2008**, 136, 3-10.
22. International Maritime Organization (IMO). Prevention of air pollution from ships. MEPC 57/21, April 2008, pp.28-57.
23. Rehmatullaa, N.; Calleyab, J.; Smitha, T. The implementation of technical energy efficiency and CO2 emission reduction measures in shipping, *Ocean Engineering*, **2017**, 139, 184-197.
24. Benajes, J.; Molina, S. A.; Garcia, J. M. Influence of pre- and post-injection on the performance and pollutant emissions in a HD diesel engine. *SAE technical paper* **2001**, 2001-01-0526.
25. Ishikawa, N.; Uekusa, T.; Nakada, T.; Hariyoshi, R. DI diesel emission control by optimized fuel injection. *SAE technical paper* **2004**, 2004-01-0117.
26. Payri, F.; Benajes, J.; Pastor, J. V.; Molina, S. Influence of the post-injection pattern on performance, soot and NOx emissions in a HD diesel engine. *SAE technical paper,* 2002, 2002-01-0502.
27. Chryssakis, C. A.; Hagena, J. R.; Knafl, A.; Hamosfakidis, V.; Filipi, Z. S.; Assanis, D. N. In-cylinder reduction of PM and NOx emissions from diesel combustion with advanced injection strategies. *Int. J. Veh. Des*., 2006, 41, 83–102.
28. Andreadis, P.; Zompanakis, A.; Chryssakis, C.; Kaiktsis, L. Effects of the Fuel Injection Parameters on the Performance and Emissions Formation in a Large-Bore Marine Diesel Engine, *International Journal of Engine Research,* **2011**, 12, 14.
29. Hu, Y.; Yang, J.; Hu, N. Experimental Study and Optimization in the Layouts and the Structure of the HPCR Fuel Injection System for a Marine Diesel Engine, *International Journal of Engine Research,* **2020**, 22(6).
30. Balz, R.; Rotz, B.; Sedarsky, D. In-nozzle flow and spray characteristics of large two-stroke marine diesel fuel injectors, *Applied Thermal Engineering*, **2020,** 180.
31. Wang, G.; Yu, W.; Yu, Z.; Li, X. Study on Characteristics Optimization of Combustion and Fuel Injection of Marine Diesel Engine, *Atmosphere* 2022, 13, 1301.
32. Balz, R.; Bernardasci, G.; Rotz, B,; Sedarsky, D. Influence of nozzle geometry on spray and combustion characteristics related to large two-stroke engine fuel injection systems, *Fuel*, **2021**, 294.
33. Stephenson, P.; Rutland, C. Modeling the Effects of Intake Flow Characteristics on Diesel Engine Combustion, *SAE Technical Paper* 950282, 1995.
34. Singh, S.; Reitz, R.D.; Musculus, M.P.B. Validation of engine combustion models against detailed in-cylinder optical diagnostics data for a heavy-duty compression-ignition engine, *International Journal of Engine Research*, **2007**, 8, 1.
35. O'Rourke, P.J.; Amsden, A.A. A Spray/Wall Interaction Submodel for the KIVA-3 Wall Film Model, *SAE Transactions Vol. 109, SECTION 3: JOURNAL OF ENGINES*, **2000**, 281-298.

36. Kong, S.C.; Han, Z.; Reitz, R.D. The Development and Application of a Diesel Ignition and Combustion Model for Multidimensional Engine Simulation, *SAE Transactions, Vol. 104, Section 3: JOURNAL OF ENGINES*,**1995**, 502-518.
37. Singh, S.; Reitz, R.D.; Wickman, D.; Stanton, D.; Tan, Z. Development of a Hybrid, Auto-Ignition/Flame-Propagation Model and Validation Against Engine Experiments and Flame Liftoff, *SAE Transactions Vol. 116, Section 3: JOURNAL OF ENGINES*, **2007**, 176-194.
38. Patterson, M.A.; Kong, S.C.; Hampson, G.J.; Reitz, R.D. Modeling the Effects of Fuel Injection Characteristics on Diesel Engine Soot and NOx Emissions, *SAE Transactions, Vol. 103, Section 3: JOURNAL OF ENGINES*, **1994**, 836-852.
39. Torres, D.J.; Li , Y.H.; Kong, S.C. Partitioning strategies for parallel KIVA-4 engine simulations, *Computers & Fluids*, **2010**, 39 , 301–309.
40. Torres, D.J.; Trujillo, M.F. KIVA-4: An unstructured ALE code for compressible gas flow with sprays, *Journal of Computational Physics*, **2006**, 219, 943–975.
41. Imamori, Y.; Hiraoka, K.; Murakami, S.; Endo, H.; Rutland, C.J.; Reitz, R.D. Effect of mesh structure in the KIVA-4 code with a less mesh dependent spray model for DI diesel engine simulations, *International Multidimensional Engine Modeling User's Group Meeting at the SAE Congress*, **2009**.
42. Sone, K.; Menon, S. Effect of Subgrid Modeling on the In-Cylinder Unsteady Mixing Process in a Direct Injection Engine, *Journal of Engineering for Gas Turbines and Power*, **2003**, 125, 435-443.
43. Yang, S.L.; Siow, Y.K.; Teo, C.Y.; Hanjalic, K. A KIVA code with Reynolds-stress model for engine flow simulation, *Energy*, 2005, 30, 427–445.
44. Reitz, R.D.; Rutland, C.J. DEVELOPMENT AND TESTING OF DIESEL ENGINE CFD MODELS, Prq Energy Cumhusr. Sri. 1995, 21, 173-196.
45. Maghbouli, A.; Yang, W.; An, H.; Li, J.; Chou, S.K.; Chua, K.J. An advanced combustion model coupled with detailed chemical reaction mechanism for D.I diesel engine simulation, Applied Energy 2013, 111, 758–770.
46. Mattarellia, E.; Rinaldinia, C.A.; Golovitchevb, V.I. CFD-3D analysis of a light duty Dual Fuel (Diesel/Natural Gas) combustion engine, Energy Procedia, 2014, 45, 929 – 937.
47. Jeong, Y.I.; Qian, Y.; Campbell, S.; Rhee, K.T. Investigation of a Direct Injection Diesel Engine by High-Speed Spectral IR Imaging and KIVA-II, SAE Transactions Vol. 103, Section 3: JOURNAL OF ENGINES, 1994, 1789-1799.
48. Imren, A.; Golovitchev, V.; Sorusbay, C.; Valentino, G. The Full Cycle HD Diesel Engine Simulations Using KIVA-4 Code, SAE 2010 Powertrains Fuels & Lubricants Meeting, San Diego California, United States 2010.
49. Wickman, D,; Senecal, P,; Reitz, R.D, Diesel Engine Combustion Chamber Geometry Optimization Using Genetic Algorithms and Multi-Dimensional Spray and Combustion Modeling, SAE 2001 World Congress, Detroit Michigan, United States, 2000.
50. Tsao, K.; Dong, Y.; Xu, Y. Investigation of Flow Field and Fuel Spray in a Direct. Injection Diesel Engine via KIVA-II Program, SAE Technical Paper 901616, 1990.
51. Hyun, G.; Lee, D.; Goto, S. KIVA Simulation for Mixture Formation Processes in an In-Cylinder Injected LPG SI Engine, SAE Technical Paper 2000-01-2805, 2000.
52. Mariani, F.; Postrioti, L. Modeling Diesel Engine Using KIVA II 3D-Code: Validation of a New Global Combustion Model and its Sensitivity to the Spatial Discretization, SAE Transactions Vol. 105, Section 3: JOURNAL OF ENGINES, 1996, 1359-1366.
53. Naik, S.; Ramadan, B. A Numerical Study and Optimization of GDI Engine Parameters for Better Performance and Complete Combustion Using KIVA-3V and VISUALDOC®, SAE Technical Paper 2004-01-3008, 2004.
54. Amsden, A.A.; O'Rourke, P.J.; Butler, T.D. KIVA-II: A Computer Program for Chemically Reactive Flows with Sprays, LA-11560-MS UC-96, 1989.